The Pennsylvania State University

The Graduate School

College of Engineering

LOW-EARTH-ORBIT TARGET DESIGN FOR

OPTICAL CALIBRATION OF THE FALCON TELESCOPE NETWORK

A Thesis in

Aerospace Engineering

by

Heather C. Nelson

Submitted in Partial Fulfillment
of the Requirements
for the Degree of

Master of Science

December 2014

The thesis of Heather C. Nelson was reviewed and approved* by the following:

Sven G. Bilén
Associate Professor of Engineering Design, Electrical Engineering,
     and Aerospace Engineering
Thesis Co-Advisor

Timothy J. Kane
Professor of Electrical Engineering and Meteorology
Thesis Co-Advisor

George A. Lesieutre
Department Head, Department of Aerospace Engineering

*Signatures are on file in the Graduate School.

ABSTRACT

In an era in which the orbital space around Earth becomes increasingly crowded with debris, Space Situational Awareness is becoming more and more critical. As a result, innovative and inexpensive methods of tracking and identifying this debris are becoming increasingly popular. The Falcon Telescope Network, a set of 13 small (20-in) telescopes stationed at sites around the world, is one such solution to the issue of debris tracking and identification. The goal of this network is to determine how much information can be obtained about an object in space from the optical signature of an unresolved image.

In order to help determine how much information can be learned about a given unknown target, it is useful to have access to a target whose exact properties are known. A target that is passively controlled by a gravity-gradient boom and that has four panels with unique optical signatures (aluminized Kapton film, aluminum, gold, and pyrolitic graphite with two opposing solar panels) is the proposed initial target design for this program. In order to improve the reflection geometry, the sides of the target will fold down after deployment from the P-POD. This target will provide some degree of stabilization, as well as unique optical signatures, while minimizing costs. Future target designs can incorporate more complex stabilization techniques and communication systems that will allow for commanded attitude and exchange of attitude information.

TABLE OF CONTENTS

LIST OF ABBREVIATIONS

ADCS   Attitude Determination and Control System
AFOSR   Air Force Office of Scientific Research
AFIT   Air Force Institute of Technology
AFRL   Air Force Research Lab
ALICE   AFIT LEO iMESA CNT Experiment
AMOS   Air Force Maui Optical Station
AO   Atomic Oxygen
AU   Astronomical Units
CCD   Charged-Coupled Device
CNT   Carbon Nanotube
COTS   Commercial Off-The-Shelf
DARPA   Defense Advanced Research Projects Agency
FTN   Falcon Telescope Network
GEO   Geosynchronous Earth Orbit
HF   High Frequency
iMESA   Integrated Miniaturized Electrostatic Analyzer
ISIS   Innovative Solutions In Space
ISS   International Space Station
LCS   Lincoln Calibration Sphere
LEO   Low Earth Orbit
MEO   Middle Earth Orbit
MISSE   Materials International Space Station Experiments
NASA   National Aeronautics and Space Administration
NRL   Naval Research Laboratory
NRO   National Reconnaissance Organization
NSF   National Science Foundation
PEACE   Polymer Erosion and Contamination Experiment
PERCS   Precision Expandable Radar Calibration Target
PMAC   Passive Magnetic Attitude Control
P-POD   Poly Picosatellite Orbital Deployer
RCOS   Ritchey–Chretien Optical Systems
RMS   Root Mean Square
SRP   Solar Radiation Pressure
STP   Space Test Program
SURCAL   Surveillance Calibration
USAFA   United States Air Force Academy

LIST OF SYMBOLS

δ	Collapsed side panel angle
ζ	Zenith angle
θ	Angular resolution
θ_i	Angle of incidence
θ_r	Angle of reflection
θ_s	Satellite attitude angle
λ	Wavelength
λ_B	Magnetic latitude factor
μ	Earth's standard gravitational parameter
ν	Frequency of light
ρ	Mean atmospheric density
ϕ	Solar constant
ω	Tracking speed
c	Speed of light in a vacuum
cm	Center of mass
cp_s	Canter of solar pressure
h	Height above optic
m	Satellite mass
r	Altitude of satellite
r_0	Fried parameter
s	Separation distance (arc length)
t_{orb}	Orbital lifetime
q	Reflectance factor
A	Cross-sectional area
A_l	Lens area
A_s	Sunlit surface area
B	Residual dipole moment
C_D	Drag coefficient
C_n	Refractive index structure constant
D	Aperture diameter
E_{photon}	Energy of a single photon
F_G	Reflected solar flux that reaches Earth's surface
F_R	Reflected solar flux at the satellite surface
I_y	Moment of inertia about y-axis
I_z	Moment of inertia about z-axis
P	Photons detected per pixel per microsecond
$Q.\,E.$	Quantum efficiency
R	Distance from center of Earth to satellite
T	Orbital period
T_a	Atmospheric drag torque
T_g	Gravity-gradient torque
T_m	Magnetic torque
T_s	Solar radiation pressure torque
V	Orbital speed

LIST OF FIGURES

LIST OF TABLES

ACKNOWLEDGMENTS

Chapter 1: Introduction

Problem Statement

As the United States and other space-faring nations close out the sixth decade of manned and unmanned presence in space, we are becoming plagued by the very technology that has gotten us this far. Space is becoming increasingly crowded by both space junk (dead satellites, debris, etc.) and operational spacecraft. Space junk is particularly problematic in low Earth orbit (LEO), which is an altitude used for many missions. However, the crowding of LEO also poses a threat to spacecraft that must pass through LEO on their way to medium Earth orbit (MEO) and geosynchronous Earth orbit (GEO).

For this reason, the tracking and monitoring of both space junk and operational satellites is of great concern to both the United States and the U.S. Air Force, and has been for many years. Events such as China's 2007 intentional destruction of a satellite with a kinetic kill vehicle, as well as the increasing frequency of collisions and near collisions of satellites and debris on a regular basis, increase the need for more in-depth tracking. The debris that results from these events remains in orbit until it burns up in Earth's atmosphere, which can take many decades and is an incredibly variable and somewhat unpredictable process. The United States already performs detailed monitoring of the positions of many thousands of satellites and pieces of debris in orbit, but this data is largely position based and does not, for the most part, include imaging. [1]

There are essentially two strategies for ground-based imaging of such a variety of objects. The first is to create ever larger and faster telescopes capable of tracking both small satellites (and debris) moving quickly in LEO and large satellites moving more slowly in GEO. However, the price of glass optics increases exponentially with their size, and a larger size also results in the weight of the optic being greater. Heavy optics are more difficult to move at the fast tracking speeds and with the precision required to track the wide range of satellites. The second option is to create a widespread network of smaller telescopes that are capable of high speed, albeit lower resolution, tracking whose lower resolution data can be used to infer some information about the objects they can see. The Falcon Telescope Network (FTN) is this second solution. [1]

The FTN consists of 13, 20–in f/8.1 telescopes placed at locations around the globe. This global network of telescopes is capable of conducting simultaneous observations of the same object under different lighting conditions, which an Air Force Office of Scientific Research (AFOSR) investigation has shown to have great photometry benefits. An added benefit of the FTN is that all the hardware and software are available as commercial off-the-shelf (COTS) components, which saves a tremendous amount of money that would otherwise have to be spent on research and development. As a result, the unit cost for each FTN site is only about $157,000. [1]

Telescope Specifications

The telescopes used for the FTN are RC Optical Systems, 20–in f/8.1 Carbon Truss Ritchey–Chretien Telescopes (seen in Figure 1). These telescopes are available for use in the FTN without modification. They are tested and certified to at least 1/20th wavelength RMS and have an enhanced aluminum overcoat with 96.9% reflectivity. [2]
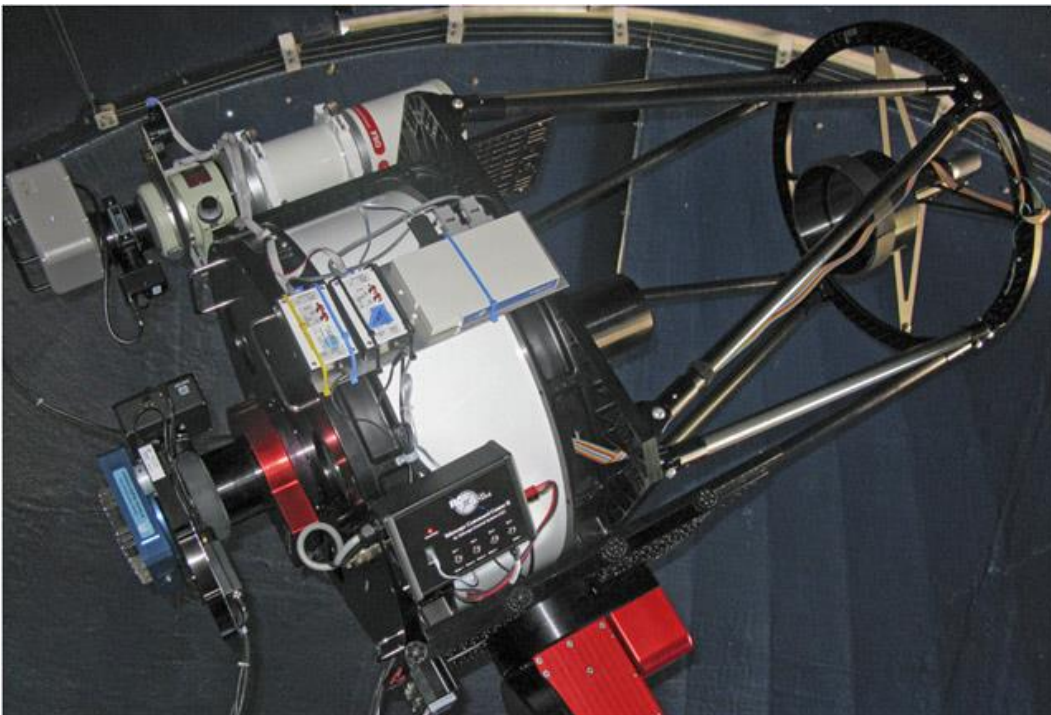
Figure 1: RCOS 20–in f/8.1 Telescope

The FTN utilizes an Apogee Alta F47-MB (mid-band) high-performance, cooled CCD camera system. The specifications for this CCD are summarized in Table 1. The CCD for this camera system is most efficient in the visible light spectrum (as seen in Figure 2, displayed in red). In addition to the specifications of the CCD, the specifications of the entire camera system are also important for determining the performance expectations of the FTN. Some important system specifications for this camera can be found in Table 2. [3]

Table 1: Apogee Alta F47 CCD Specifications

CCD	E2V CCD47-10
Array Size (pixels)	1024×1024
Pixel Size	13×13 microns
Imaging Area	13.3×13.3 mm (177 mm^2)
Dynamic Range	83 dB
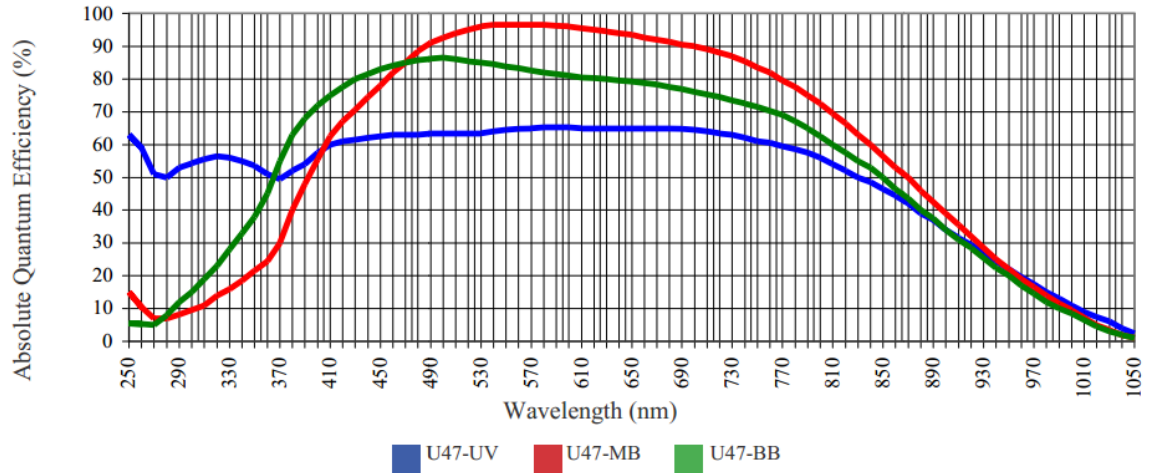
Figure 2: Apogee Alta F47 CCD Sensitivity [3]

Table 2: Apogee Alta F47 Camera System Specifications

Digital resolution	16 bits at 1 and 4 MHz
System noise (typical)	15 e$^-$ RMS at 1 MHz
Pixel binning	1×1 to 8×1024 on-chip
Exposure time	30 ms to 183 min (2.56-ms increments)
Temperature stability	± 0.1 °C
Operating environment	−25 to 40 °C, relative humidity 10–90%
Plate scale	50 arcseconds/mm (242.41 microradians/mm)
Field of view	660 arcseconds (3199.77 microradians)

Telescope Locations

Each of the FTN telescope systems will be placed in one of 12 different locations: Colorado Mesa University (Grand Junction, CO); Fort Lewis College (Durango, CO); Northeastern Junior College (Sterling, CO); Otero Junior College (La Junta, CO); Pennsylvania State University (University Park, PA); Universidad de La Serena (La Serena, Chile); Observatorio Mamalluca (Vicuña, Chile); University of Queensland (Brisbane, Australia); University of New South Wales Australia (Sydney, Australia); and Kauai Community College (Kauai, HI), as well as yet-to-be-determined locations in South Africa and Europe. These sites can be seen in Figure 3 (which has been adapted from an early USAFA FTN Poster).
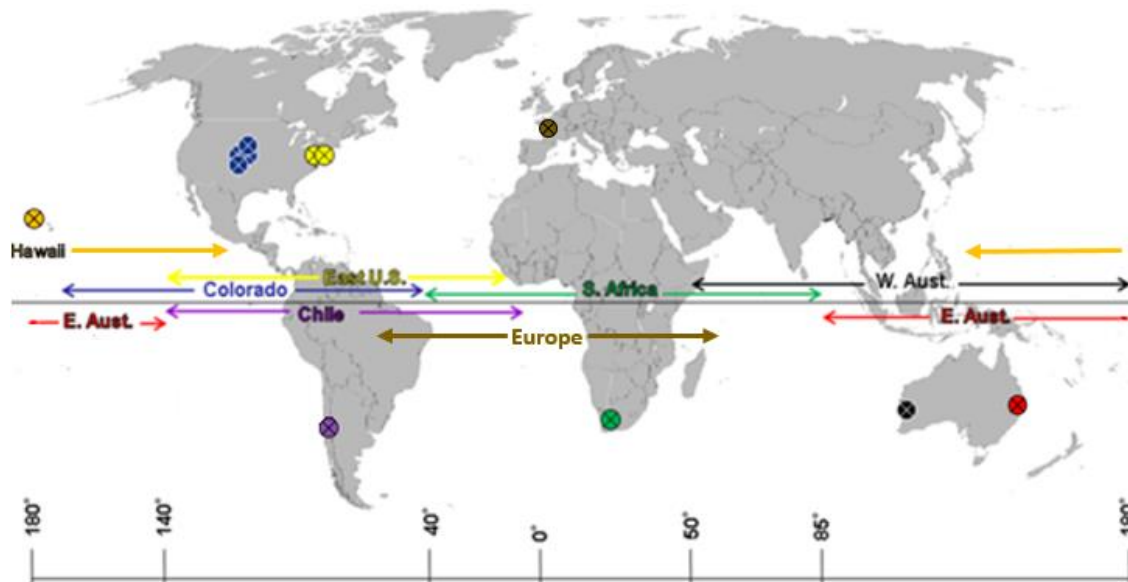
Figure 3: Locations of Fixed Sites for the FTN and Approximate Ground Station Coverage for Geosynchronous Orbit

Thesis Contributions

Contributions of this thesis are an analysis of the resolution of the FTN telescopes, initial calculation of FTN telescope light-intensity requirements, a morphological discussion of possible calibration targets for the FTN, comparison of said designs to a selected proposal, as well as an analysis of material choices and their expected optical signatures.

Thesis Overview

Chapter 2 of this thesis discusses previous, and ongoing, space-based calibration campaigns for optical, laser, and radar calibration. Chapter 2 also includes a discussion of the history of CubeSat development and the use of these satellites in Air Force applications. Finally, chapter 2 contains brief calculations and analysis of various orbital regimes and environmental perturbations.

Chapter 3 is a review of basic imaging theory, in particular, the diffraction limit and Fried parameter of an optic and atmospheric effects on imaging. This review is related to the imaging goals of the FTN and how they will effect target detection.

Chapter 4 contains an overview of each of the design proposal categories and a brief description of each of the categories, as well as a description of each design within the various categories.

Chapter 5 discusses the design comparison, elimination, and eventual selection of a calibration target design. The chapter also contains a detailed discussion of the chosen target and considerations that must be made in target development. The final sections of Chapter 5 are a discussion of materials to be used in the calibration target design, as well as the optical signature that can be expected from each of these materials.

The final chapter, Chapter 6, includes the final design recommendation and recommendations for future work to be done.

Chapter 2: Background

Previous Calibration Campaigns

Satellites of various sizes have been used for decades for calibration of ground- and satellite-based systems. Calibration satellites can be used for laser, radar, or optical calibration as required by the mission. Usually, the satellites used for this purpose are spherical because spheres are the least complex geometry and the orientation of a sphere is irrelevant; regardless of the orientation, the cross-section of the target remains constant. This regularity is a highly desirable trait in a "dumb" target that lacks an Attitude Determination and Control System (ADCS).

There are a few calibration target campaigns worth discussing briefly:

1) Lincoln Calibration Sphere (LCS). The LCS is a hollow aluminum spherical satellite with "a precisely defined radar cross-section." LCS 1 and LCS 4 were successfully launched in 1965 and 1971, respectively. They have a diameter of 1.12 m and a wall thickness of 3.2 mm. Unfortunately, LCS 2 and LCS 3 (attempted launches in 1965 and 1968) were both lost due to launch failure. The optical cross-section of the LCS satellites is 1 m^2 (assuming 100% reflection). Both LCS 1 and LCS 4 are still in use as radar calibration targets today. LCS 1 is in a 2700-km circular orbit with a predicted lifetime of 30,000 years. LCS 4 is in a "low Earth orbit with a lifetime of about 75 years." [4]

2) Surveillance Calibration Satellites (SURCAL). SURCAL is a radar calibration program for the U.S. Air Force and other approved U.S. entities. The SURCAL program consists of 15 U.S. Air Force target satellites of varying masses and dimensions. The exact properties of all of these satellites are not publicly available, but two of them, SURCAL 160 and SURCAL 150B, are spheres with a mass of 2.00 kg and have diameters of 20 in and 16 in, respectively. The first SURCAL satellite, SURCAL 1A (37 kg mass), launched in 1962 and decayed in 1966. SURCAL 2A (3 kg mass), which was on the same launch, decayed in 1963. The last SURCAL launch was in 1969 and launched four satellites; however, the decay dates for these satellites are not publicly available. [5]

3) Precision Expandable Radar Calibration Target (PERCS). PERCS has completed construction but is awaiting a launch opportunity. PERCS was developed by the Naval Research Laboratory (NRL), together with Hoberman Associates of New York. The expandable PERCS satellite is a large Hoberman sphere, which has a collapsed (stored) diameter of 1.25 m and an expanded diameter of 10.2 m. The PERCS sphere consists of 180 vertices and 360 edges and provides a radar cross-section of approximately 200 m^2 at HF. Each vertex is outfitted with a corner-cube retroreflector on both the inside and outside of the frame that allows for calibration of laser satellite tracking. The primary purpose of PERCS is to calibrate high frequency (3–30 MHz) backscatter radar used for space weather studies of the upper atmosphere. [6]

4) Starshine. Starshine was conceived of by the U.S. Naval Research Laboratory but has been built by a team of organizations that received no funding and whose members volunteered their time. NASA placed three Starshine satellites into highly inclined Earth orbits at no cost to the Starshine program itself. Starshine 1 was deployed from Space Shuttle Discovery in June 1999 in a 387-km, 51.6° inclined orbit. Starshine 1 is a 48-cm-diameter sphere covered in 878, 1-in-diameter polished aluminum mirrors. Starshine 1 deorbited in February 2000 after eight months in orbit. Starshine 2 deployed in December 2001 from Space Shuttle Endeavor into a 370-km, 51.6° inclined orbit. Similar to Starshine 1, Starshine 2 had 858 polished mirrors, but it also included 31 laser retro-reflectors. Starshine 2 deorbited in April 2002 after only four months. Starshine 2 had a shorter lifetime than Starshine 1 due to lower deployment altitude and high solar activity. Starshine 3 also launched in September 2001 but into a 470-km, 67° inclined orbit from an Athena I rocket out of Kodiak, Alaska. Starshine 3 was significantly larger than the other two at 37–in in diameter. Because of its larger size, Starshine 3 carried 1500 polished mirrors and 31 laser retro-reflectors. Starshine 3 deorbited in January 2003. The primary mission of the Starshine program is optical calibration. The Starshine satellites were visible (even to the naked eye in the right conditions) to more than 66% of Earth while they were in orbit. In addition

to their mission of optical calibration, the latter two Starshine satellites also had laser targets to perform laser ranging calibration missions. [7]

In order to maintain the low cost of the FTN, one economically feasible solution for calibration of the FTN is to use CubeSats. From a cross-section perspective, cube-shaped CubeSats are not ideal because the orientation of a cube matters, whereas a sphere's orientation does not. There is no standardized, spherical, picosatellite design like there is for CubeSats. However, that is not necessarily a limitation. It is possible to change the shape of the CubeSat once in orbit to make the reflection geometry more favorable.

Under the assumption that cubes are to be used instead of spheres, two options remain. The first option is a "dumb" satellite that does not have ADCS. These satellites are comparatively inexpensive because they lack the more-complex components that would otherwise drive up costs. On the other hand, there is an element of the unknown when there is limited to no control over the attitude of the satellite. Lack of knowledge about the attitude of the target is a concern from a calibration standpoint. The second option is a "smart" satellite that does have ADCS. This option is significantly more costly, but there is the added benefit of knowing, and being able to control, the satellite's attitude at all times.

CubeSat History

CubeSats were first developed in 1999 at the California Polytechnic State University [8]. The purpose for the development of CubeSat technology was to develop "a new class of standardized picosatellites" that can take advantage of technology that allows standard satellite components to be made smaller and smaller. Cal Poly developed both a size and mass standard for the picosatellites, as well as a standardized launcher called a Poly Picosatellite Orbital Deployer (P-POD). The standardization of this technology further helps to drive down the cost of development for each picosatellite. [9]

The initial development of CubeSat technology by Cal Poly was for a 100-mm-per-side cube picosatellite with a maximum mass of 1 kg (what has now become known as a 1U CubeSat). The 1U (also known as "one unit CubeSat" or "cube") is

approximately 10×10×10 cm in size and now allowed 1.33 kg or less in mass. Since that initial development, larger CubeSats have been created, including 2U (or "double cube") which is about 10×10×20 cm and 3U (or "triple cube"), which measures approximately 10×10×30 cm. More details and sample models of each type of CubeSat can be found in Table 3. [8]

As CubeSats continue to prove themselves as an effective technology, there is interest in larger and larger CubeSat designs. (Although larger than the original CubeSat designs, these larger CubeSats are still smaller than their "small sat" relatives of earlier generations, which measure closer to 1 m^2 on a side.) These designs are currently under development with the Space Test Program (STP) and Air Force Research Lab (AFRL) and include 6U, 12U, and 27U. More details and sample models of each type of these larger CubeSat designs can be found in Table 4. [10]

Table 3: Specifications for 1U, 2U, and 3U CubeSats
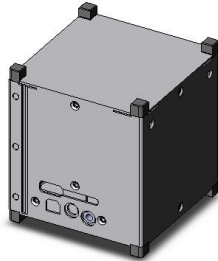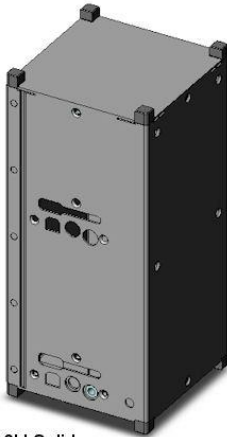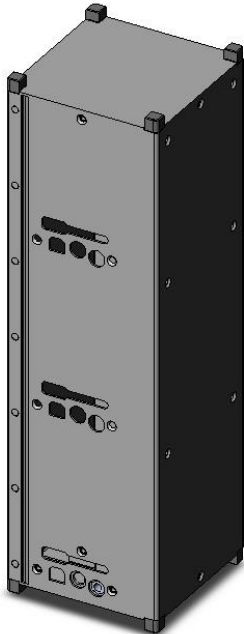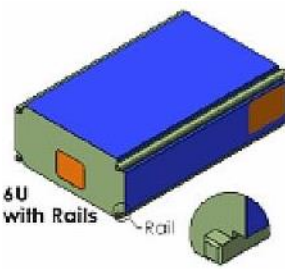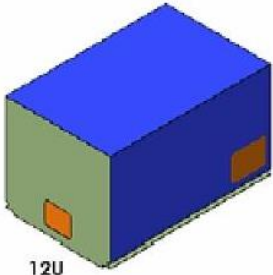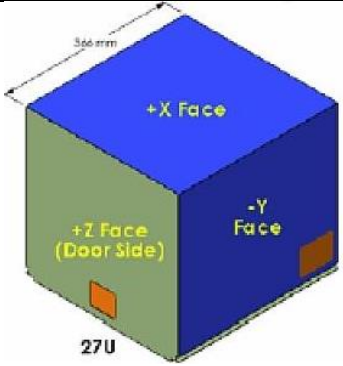
	1U CubeSat	2U CubeSat	3U CubeSat
CAD Model [11]	1U Solid CAD Model RevD	2U Solid CAD Model RevD	3U Solid CAD Model RevD
Dimensions (cm)	10.0±0.01 in X,Y 11.4±0.01 in Z	10.0±0.01 in X,Y 22.7±0.02 in Z	10.0±0.01 in X,Y 34.5±0.03 in Z
Max Mass (kg)	1.33	2.66	4.00

Table 4: Specifications for 6U, 12U, and 27U CubeSats

	6U CubeSat	12U CubeSat	27U CubeSat
CAD Design [10]			
Dimensions (cm)	12.0 in X 24.0 in Y 36.0 in Z	23.0 in X 24.0 in Y 36.0 in Z	34.0 in X 35.0 in Y 36.0 in Z
Max Mass (kg)	12.00	24.00	54.00

These larger CubeSat designs cannot fit into the standard P-POD launcher (Figure 4) developed by Cal Poly so other launchers are under development by various companies, in a number of countries, to accommodate the larger designs. Alternative launchers also exist for all current CubeSat sizes. These launchers are considered complementary to, rather than competitors of, the P-POD and often present their own advantages over the P-POD. However, the P-POD continues to be a popular choice for picosatellite missions. The P-POD and other launch systems for CubeSats traditionally launch according to a secondary payload model, which can also be seen in Figure 4. [10] The P-POD deploys the CubeSats with a spring in the base of the P-POD. When the door is triggered to open, the CubeSat slides out along the rails inside the P-POD and should, in theory, be released with very minimal torque or spin. In a perfect scenario, the CubeSat is released straight from the P-POD perfectly stable with no initial conditions. In reality, initial conditions will be imparted on the satellite from both the launch vehicle residual motion as well as P-POD tip off (misalignment of the spring, imperfect insertion of the satellite in the P-POD, etc.). If the CubeSat is released with an initial rate of spin, and the CubeSat has the required systems to do so, it may correct for this initial condition, using its ADCS, 30 minutes after release from the P-POD to ensure it has cleared the launch vehicle and any other payloads that may have been released nearby. [8]
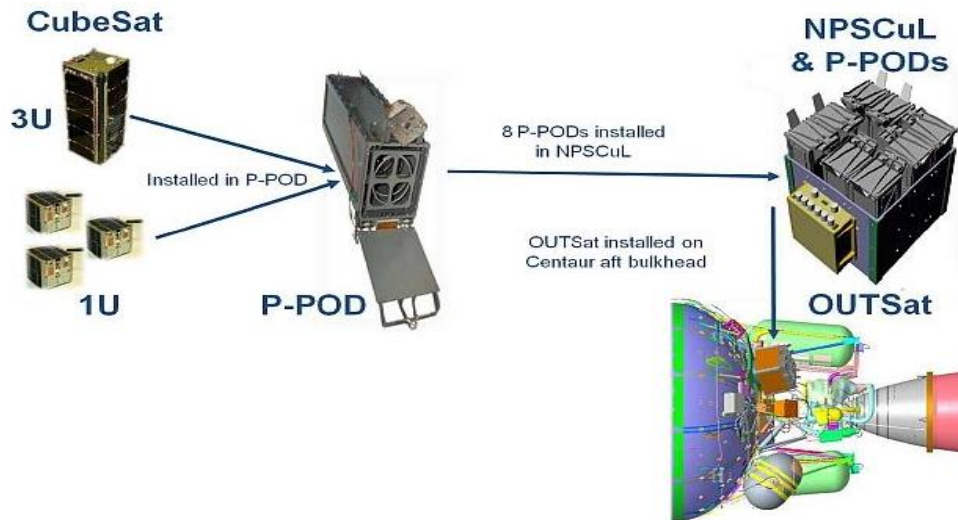
Figure 4: Example of P-POD and P-POD Packing and Placement Scheme for the Atlas-5 Rideshare System

CubeSats have the potential to enable great leaps in space technology while simultaneously saving significant amounts of money over their full-size, non-standard counterparts. For this reason, many agencies, including the National Science Foundation (NSF), the National Aeronautics and Space Administration (NASA), the Space Test Program (STP), the National Reconnaissance Organization (NRO), and the Defense Advanced Research Projects Agency (DARPA), currently fund various aspects of CubeSat development programs in a competitive environment. By competing for funding and launches, CubeSat researchers and developers are pushing the limits of possibility for the technology and are finding more and more creative ways to make use of the limited space available onboard.

The U.S. Air Force has begun to experiment with CubeSat technology as well. On 12 June 2013, AFIT LEO iMESA CNT Experiment (ALICE) was launched. This picosatellite was the first of the U.S. Air Force's CubeSats and was developed by graduate students and staff at the Air Force Institute of Technology (AFIT) with a 3U bus provided by the NRO. [12] Unfortunately, a malfunction with the bus prevented the solar panels from deploying and ALICE lost power shortly after deployment from the P-POD. [13] Around the same time, the NRO also chose to provide a 3U bus to the United States Air Force Academy (USAFA) for the development of FalconSAT-7. The primary payload onboard FalconSAT-7 is a deployable photon sieve telescope, funded by

11

DARPA. FalconSAT-7 is scheduled to launch in May 2016. [14] The development budget provided to USAFA by DARPA for FalconSAT-7 is $1.8 million. Almost all of this cost is directly applied to research, development, and construction, since the program uses an existing ground station network and other existing measures to limit development costs. Without these resources available, total project cost would increase dramatically. [13] (Contrary to what the names might indicate, FalconSAT-7 is not directly related to the FTN except that they are both USAFA programs; many USAFA-based programs use the school mascot, the Falcon, as their namesake.) These two CubeSat programs represent the totality of current U.S. Air Force CubeSat projects. However, CubeSats are a fairly recent technology and the current interests of the U.S. Air Force play very strongly into the strengths of CubeSats. For this reason, there will likely be a surge of CubeSat use in the U.S. Air Force in coming years.

One of these anticipated future uses of U.S. Air Force CubeSats should be the calibration of the FTN. Calibration of the network aids in the algorithm used to refine the images gathered by the many telescope sites. Since the goal of the FTN program is to track and identify both known and unknown space objects, it is beneficial to have a CubeSat, or network of CubeSats, with known location and properties to observe and calibrate the system. Since the FTN program is one that is focused on exploiting COTS components in order to reduce program costs, it only makes sense to utilize CubeSats, which are the closest thing to a COTS satellite, for the calibration of the system. It would hardly make sense to spend as much on a calibration mechanism as on the rest of the program combined.

Orbital Mechanics

In order to determine the best design for the mission of calibration, it was necessary to take into consideration the orbital mechanics properties for satellites at various altitudes. Each orbital regime—LEO, MEO, and GEO—presents advantages and disadvantages. For the purposes of this basic analysis, each orbit was assumed to be circular (eccentricity of zero). Before deciding on the right orbit for the mission design, it was first necessary to determine the properties of each orbital regime. These properties

were determined with a few quick calculations. First, the orbital speed of a circular orbit was calculated by

$$V = \sqrt{\frac{\mu}{R}}, \tag{1}$$

where μ is the standard gravitational parameter (398600.5 km³/s² for Earth) and R is the distance from the center of Earth to the satellite (the radius of Earth plus the altitude of the orbit). Next, the orbital period of the satellite (for circular orbits) was calculated using

$$T = 2\pi \sqrt{\frac{8R^3}{\mu}}. \tag{2}$$

The angular resolution of the satellite in radians is the same for any orbital altitude since it is not dependent on altitude but on the wavelength of light and the aperture of the optics. This relationship is given by

$$\theta = 1.22 \left(\frac{\lambda}{D}\right). \tag{3}$$

The wavelength of light that the telescope observes is λ and D is the diameter of the primary optic of the telescope (in the same units as wavelength). It should be noted that this equation assumes a perfect situation with no atmospheric disturbance, vibration, or other perturbing effects, which may or may not be present. For this reason, this number represents the best case value for each situation and, in reality, the angular resolution will be larger than these calculated values. Since the FTN operates in the visible light spectrum, a wavelength of 550 nm (the center of the visible light spectrum) was used for calculations. The diameter of the primary optic in the FTN telescopes is 20 in. Once the angular resolution was calculated in radians, the separation distance necessary for the telescope to distinguish between two different objects was found using

$$s = r\theta, \tag{4}$$

where r is the altitude of the satellite (distance from the surface of Earth to the satellite). Finally, the tracking speed required of the telescope to track an object in each orbital regime is calculated using

$$\omega = \frac{V}{r}. \tag{5}$$

Table 5 shows the results of these calculations for each of the three orbital regimes.

Table 5: Orbital Mechanics Properties of Various Orbital Altitudes

	LEO	MEO	GEO
Altitude, r (km)	160–2,000	2,000–35,786	35,786
Ground speed, V (km/s)	7.81–6.9	6.9–3.07	3.07
Period, T (hours)	1.47–2	2–24	24
Separation distance, s (m)	0.21–2.6	2.6–47.27	47.27
Tracking speed, ω (rad/min)	2.929–0.207	0.207–0.00515	0.00515
Tracking speed, ω (arcsec/min)	6.04×10^5–4.27×10^4	4.27×10^4–1.06×10^3	1.06×10^3

Another critical aspect of the analysis of the orbital mechanics was the lifetime of the target in orbit. Any satellite launched into LEO must have a post-mission lifetime of less than 25 years to mitigate against the buildup of space debris. In order to estimate the lifetime of the target, a calculation spreadsheet provided by the Space Test Program was used. [13] Some assumptions utilized were that the drag coefficient of the satellite is 1.05 (the drag coefficient of a cube [15]), that the mass of the satellite is the maximum allowed for the particular CubeSat size (4 kg for 1U and 50 kg for 27U), and that the F10.7 (10.7-cm radio flux) was 75 sfu (sfu = $10^{-22}\,\text{W·m}^{-2}\text{·Hz}^{-1}$), which is the predicted level for 2020. (This level is a solar minimum; over the last 65 years, 10.7-cm radio flux has varied from about 75 to 375.) [16]

Assumptions incorporated into the spreadsheet itself were that the epoch was 1 Jan 1994 at 0000 (midnight); the eccentricity was 0.005; the inclination was 28.5°; and the right ascension of the ascending node, argument of perigee, and true anomaly are all zero degrees. Additionally, the daily geomagnetic index was assumed to be 10 and the atmospheric model used was Jacchia 1971. (Although there have been updates to this model, this is the model that continues to be used by the U.S. Air Force and the Space Test Program.) Applying these assumptions, the predicted lifetime of the satellite was calculated using

$$t_{\text{orb}} = \frac{m\rho}{C_D A}, \tag{6}$$

which was imbedded in the spreadsheet provided by STP. In this calculation, m is the mass of the satellite, ρ is the mean atmospheric density, C_D is the drag coefficient and A is the area of the satellite that is in ram. Applying this equation to a variety of CubeSat sizes, the predictions for in orbit lifetime of the various satellites can be found in Table 6.

Table 6: Prediction for Time in Orbit for 1U and 27U CubeSats in LEO

Altitude (km)	1U CubeSat Time in Orbit	27U CubeSat Time in Orbit
189	11.4 days	12.7 days
250	57.4 days	64.3 days
300	238.7 days	267.5 days
350	2.4 yrs	2.7 yrs
400	8.2 yrs	9.2 yrs
450	22.0 yrs	24.6 yrs

Based on these orbital mechanical constraints, a mission orbit could begin to be determined. The first classical orbital element, the semi-major axis, must be less than or equal to 450 km in order for the spacecraft to deorbit in time to meet the 25-year-lifetime requirement. From a calibration standpoint, the most desirable eccentricity for an orbit is zero, or perfectly circular. Since it is not actually practical to get an eccentricity of exactly zero, the goal should be to get as close as possible. As for inclination, in order to be visible to the ground stations established so far, an inclination of at least 35° was required. However, the addition of a ground station in Europe will increase the required inclination since the majority of the European continent lies between 40° and 60° N latitude. For this mission, there was no real need for a specific argument of perigee or right ascension of the ascending node; therefore, the rough outline of a mission orbit was easily established.

External Torques and Disturbances

There are four primary external disturbances that affect a satellite in orbit: solar radiation pressure (SRP), atmospheric drag, magnetic torque, and gravity-gradient. Any other effects (unintended eddy currents, infrared emission pressure, outgassing, etc.) are generally either relatively small in magnitude compared to the four main forces, or only last for a limited amount of time. For these reasons, they can be considered negligible most of the time. However, in some missions, these seemingly minor effects can end up being significant as the other forces drop off; for example, this can be the case in an interplanetary mission. The relative magnitudes of these effects, as well as their regimes, are illustrated in Figure 5. [16]

For the purposes of analyzing the relative effects of these forces, it was assumed that the satellite of interest was a 27U CubeSat at full mass (54 kg), coated in a uniform

specular coating, that is symmetrical about all three axes and is launched into a 300-km orbit inclined at 79° (to align with Earth's magnetic pole [17]) in the year 2015. (While this is a practical orbit for the FTN, it also provides a common set of variables to compare various effects.)
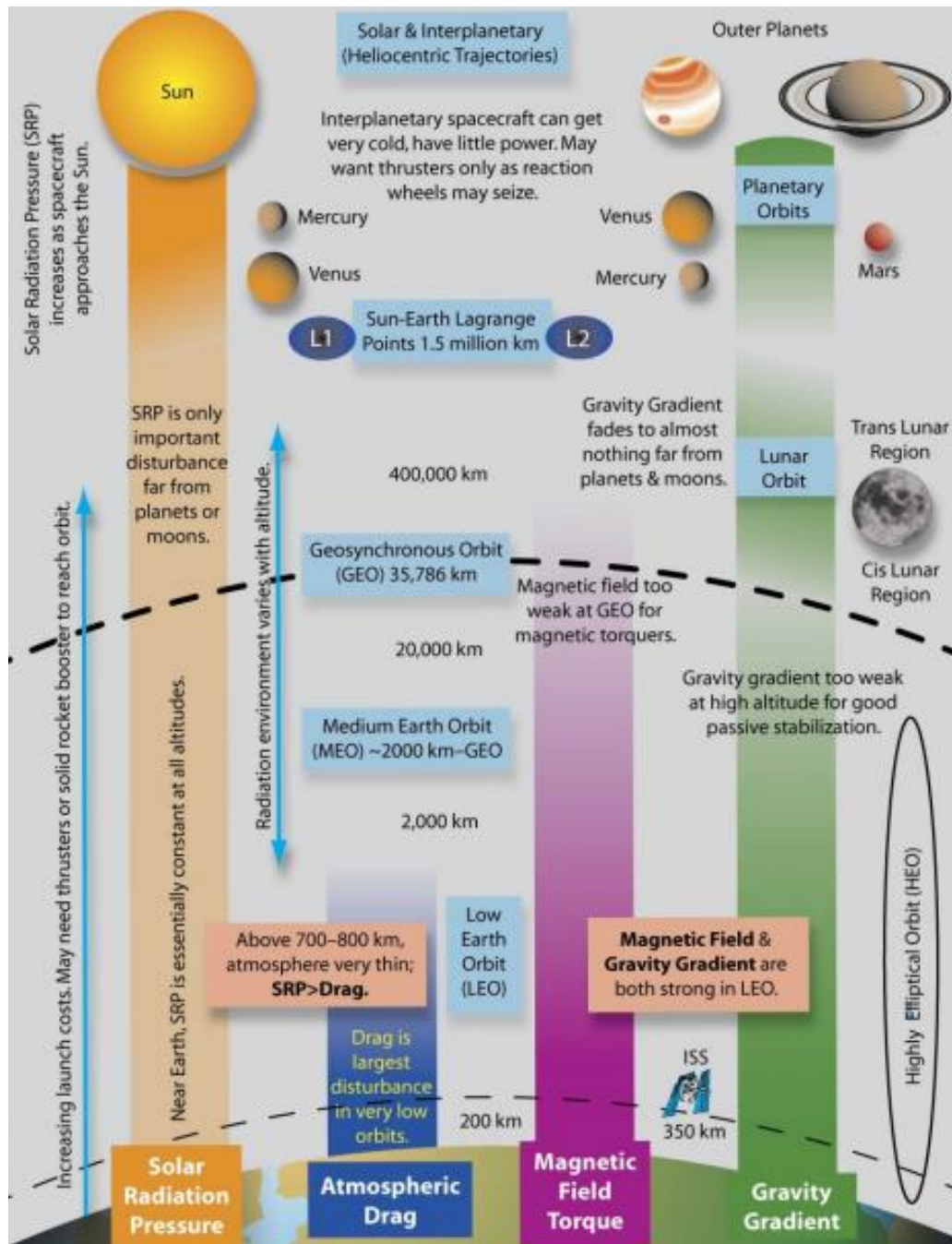
Note: Color gradient illustrates magnitude of effect; the more saturated the color, the greater the effect.

Figure 5: Effects of Major Environmental Disturbances on Spacecraft Attitude System Design. [16]

As can be seen in Figure 5 above, atmospheric drag has the largest effect on a satellite in LEO. Since this altitude is the operational regime of any calibration target for the FTN, atmospheric drag will have the greatest disturbance effect on any target that is chosen. Atmospheric drag functions in space much like it does at Earth's surface. However, atmospheric density "is roughly an exponentially decaying function of altitude," [16] meaning that the higher the altitude in the LEO regime, the less the effect of atmospheric drag will be. Above 700 to 800 km, atmospheric drag falls off significantly and SRP actually becomes a more significant effect. Atmospheric drag on a satellite was estimated using

$$T_a = \frac{1}{2}\rho C_d A_r V^2 (cp_a - cm) \,, \tag{7}$$

where T_a is atmospheric drag, ρ is atmospheric density (in kg/m^3), C_d is the drag coefficient, A_r is the ram area (in m^2), V is the orbital velocity (in m/s), and cp_a and cm are the center of aerodynamic pressure and center of mass, respectively (difference expressed in m).

A diagram of atmospheric density as a function of altitude can be found in Figure 6. Also in Figure 6, it can be seen that atmospheric density is also affected by solar weather. In solar max cycles, the atmospheric density increases.
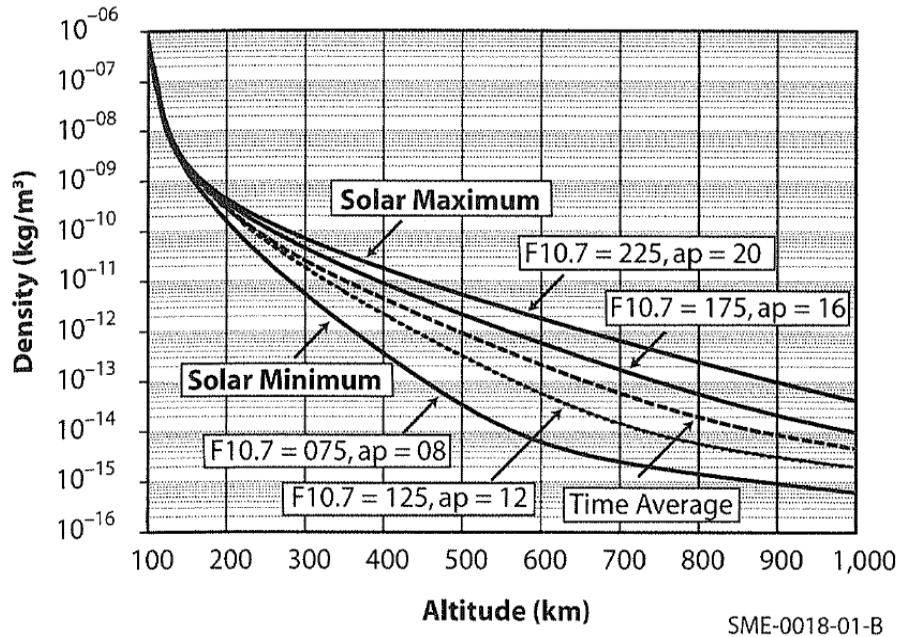
Figure 6: Density vs. Altitude for Various F10.7 Values [16]

In times of decreasing solar activity, such as Earth is currently experiencing (mid 2014) as we are past solar maximum, atmospheric density decreases, as does atmospheric drag, which results in longer orbital lifetimes of satellites. (As can be seen in Figure 8, 2014 is actually a local maximum for solar activity; however, this local maximum is still historically low.) The history of F10.7 observations, as well as predictions for future years, can be found in Figures 7 and 8, respectively.
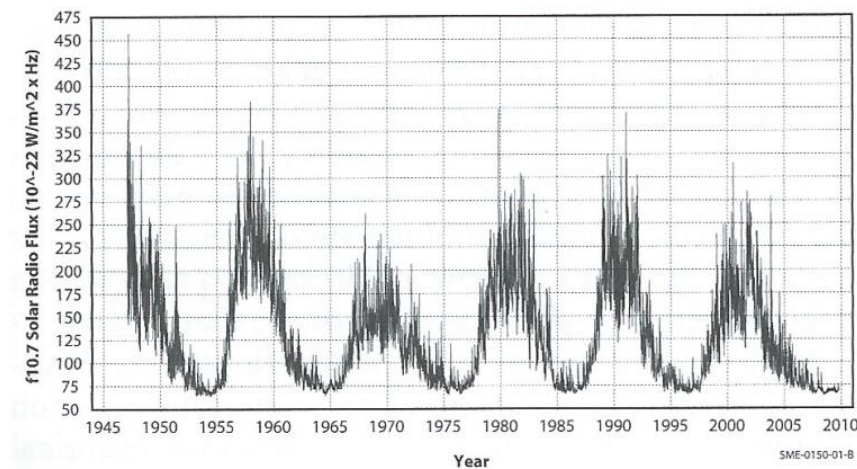
Figure 7: Observed Daily Mean Radio Flux at 10.7 cm [16]
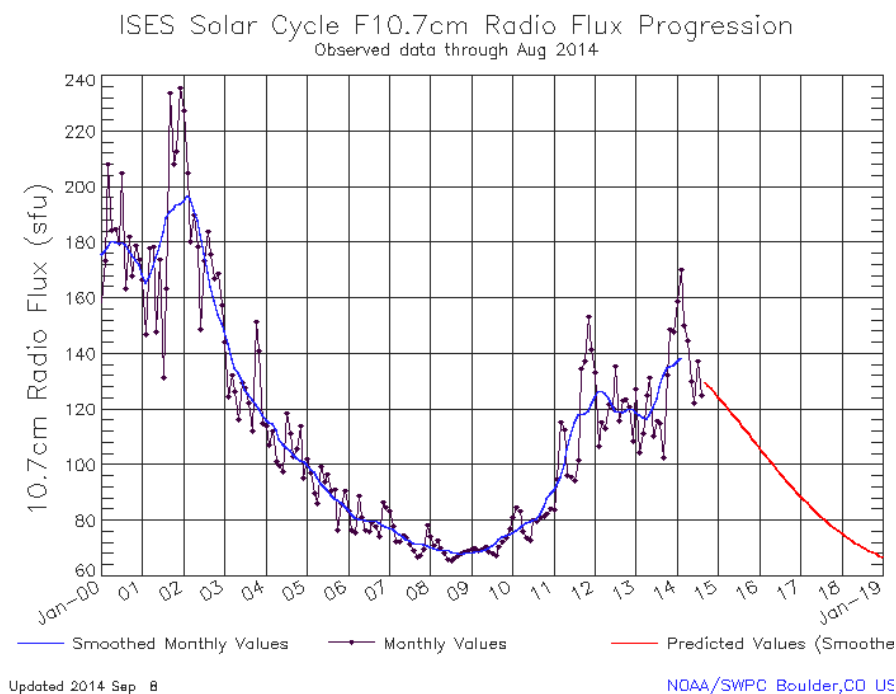
Figure 8: F10.7 Solar Cycle F10.7 cm Radio Flux Progression [18]

18

In order to analyze the example target discussed above, each component of the equation for atmospheric drag was determined. In 2015, the predicted F10.7 index is 125 sfu (see Figure 8). From Figure 6, it can be determined that the atmospheric density in 2015 for a 300-km orbit will be approximately 1.08×10^{-11} kg/m^3. (It should be noted that these solar predictions are hugely variable and may or may not be accurate. The sun is, by nature, incredibly fluid and irregular.) Next, the coefficient of drag for a cube is 1.05 when one face of the cube is in full ram (the greatest drag scenario). [18] The ram area in this scenario for a 27U CubeSat was 0.126 m^2 and the orbital velocity of a satellite at 300–km is 7,725.84 m/s. For a perfectly symmetrical spacecraft, the centers of mass and aerodynamic pressure are collocated so that was not a factor (atmospheric drag will produce a force, rather than a torque, in this case).

The next largest effect on the example satellite case is magnetic field interaction. Residual magnetic fields can exist in the satellite due to electrical components onboard, which produce a small magnetic field as the electronics function (i.e., current flows) and pass through Earth's magnetic field. As a result, "most spacecraft have some level of residual magnetic moment…[which] can range anywhere from 0.1–20 A·m^2." [16] For the purposes of analysis, it was assumed that the magnetic field was minimal, 0.1 A·m^2. The maximum magnetic torque on the satellite was calculated using

$$T_m = \frac{BM\lambda_B}{R^3},\qquad\qquad (8)$$

where T_m is the magnetic torque, B is the spacecraft residual dipole moment (in A·m^2), M is the magnetic moment of Earth multiplied by the magnetic constant ($M = 7.8 \times 10^{15}$ T-m^3), R is the distance from the satellite to the center of Earth (in m), and λ_B is "a unit-less function of the magnetic latitude that ranges from one at the magnetic equator to two at the magnetic poles." [16]

As stated before, B can be widely varying and depends largely on onboard systems. For a basic satellite like the example case that had only a coating and no onboard systems, the magnetic dipole should be minimal to non-existent. For this reason, example calculations assumed a $B = 0.1$ A·m^2 with an inclination of 79°, $\lambda_B = 2$ since the satellite was aligned with the magnetic pole. Assuming this inclination maximized the magnitude of the magnetic torque for the example case.

The next major perturbing torque is solar radiation pressure. SRP torques are particularly difficult forces to quantify because the variables in the equation change more rapidly and frequently than for the other major forces. For the example target, the satellite was uniformly coated and, therefore, all surfaces had the same reflective properties. However, for a non-uniformly coated object with an angle of incidence of zero, fully absorbing dark surfaces will absorb the momentum of the photons that strike it, while a specular white surface will reflect all of the photons that strike it, back along the same path causing the surface to experience twice the pressure force as the full absorption surface. [16] With the assumed uniform reflection, as in the example case, solar radiation pressure torque was estimated using

$$T_s = \frac{\phi}{c} A_s (1 + q)(cp_s - cm) \cos(\theta_i) \,, \tag{9}$$

where T_s is the SRP torque, ϕ is the solar constant adjusted for actual distance from the Sun (average value at the edge of the atmosphere: 1,366 W/m² at 1 AU or 149,597,871,000 m), c is the speed of light in a vacuum (3×10^8 m/s), A_s is the sunlit surface area (in m²), q is the unit-less reflectance factor (0 for perfect absorption, 1 for perfect reflection), θ_i is the angle of incidence of the sunlight upon the surface, and cp_s and cm are the centers of solar pressure and mass, respectively (difference expressed in m). [16]

In the interest of simplified calculations, it was assumed that the sunlight was directly incident upon only one side of the satellite making $A_s = 0.126$ m² and $\varphi = 0$. The example assumed perfect specular reflection, which made $q = 1$. Since the example satellite was in LEO, it was at very nearly 1 AU, so the average value for ϕ at the edge of the atmosphere can be assumed to be the value that the satellite will experience (to yield the highest possible SRP magnitude). Also, since the example was perfectly symmetrical and the sunlight was directly incident upon only one side, the difference in location of the centers of solar pressure and mass were not a factor. Again, this disturbance produced a force and not a torque.

The final perturbing effect is gravity-gradient torque. This torque is created "when a spacecraft's center of gravity is not aligned with its center of mass with respect to the local vertical." [16] For this reason, a perfectly symmetrical satellite, like the one in the example, will not experience any gravity-gradient torques. For a non-symmetrical

20

satellite, there will also be no gravity-gradient torque when the principal axis of the satellite is aligned with the local vertical. The magnitude of the gravity-gradient torque grows with increasing angle between the principal axis and the local vertical and always acts such that the torque attempts to align the two axes. [16] (While not a factor for a symmetrical satellite case, the possibility of using gravity-gradient torque as a passive control mechanism is discussed in the design section.)

For a non-symmetrical satellite, the gravity-gradient torque was approximated using

$$T_g = \frac{3\mu}{2R^3} \left| I_z - I_y \right| \sin(2\theta) ,\qquad(10)$$

which is a simplified expression for the case where the minimum principal axis is the z principal axis. [16] In this expression, T_g is the gravity-gradient torque about the x principal axis, μ is Earth's gravitational constant ($3.986{\times}10^{14}$ m^3/s^2), R is the distance from the satellite to the center of Earth (in m), θ is the angle between the local vertical and the z principal axis, and I_z and I_y are the moments of inertia about the z and y principal axes, respectively (in kg·m^2).

For the purposes of discussion, it was assumed, for this case only, that the example satellite had a difference of just 0.1 kg·m^2 between the moments of inertia about the z and y principal axes and that the x principal axis is offset from the local Earth vertical by 1°. This scenario was entirely realistic for the test case with the employment of a gravity-gradient boom. In this case, the satellite would experience a gravity-gradient torque that would attempt to realign the x principal axis with the local Earth vertical.

A summary of the magnitudes of the four main forces on the example satellite in orbit can be found in Table 7.

Table 7: Magnitude of Environmental Effects on Example Satellite

Aerodynamic Drag Force	$4.26{\times}10^{-5}$ N
Magnetic Torque	$5.24{\times}10^{-6}$ Nm
Solar Radiation Pressure Force	$1.15{\times}10^{-6}$ N
Gravity-gradient Torque	7.01 Nm

In order for another force (intended or not) to have a noticeable effect on the attitude or orbital mechanics of the satellite, it would have to exceed the magnitude of the

primary disturbances discussed above. There are a few methods of passive control that may have the ability to do just that.

1) Eddy currents. Eddy currents are created when an electric field passes through a magnetic field at high velocity. A satellite could theoretically be intentionally designed to be asymmetrical with respect to the creation of eddy currents by simply placing short conducting strips on one side of the satellite and larger strips (or a single piece) of conducting material on the opposing side. Alternatively, slots could be cut in one side to break up the conductive panels. Doing so would intentionally create a magnetic dipole on the satellite and would increase the magnetic torque. Designed properly, this could potentially give the satellite some degree of passive control, assuming the magnetic dipole created is large enough to overcome other perturbation effects on the satellite in orbit, which may or may not be possible depending on the scenario and satellite design. It could be difficult to design a large enough dipole to provide sufficient passive control. With great enough magnitude, however, this method is still only capable of providing for two axes of control.

2) Passive Magnetic Attitude Control (PMAC). This passive attitude control system "is composed of a bar magnet to supply restoring torque and a hysteresis rod to supply dampening torque." [19] This is a good solution for CubeSats specifically because it requires no power and consumes less than 50 g of the mass budget. This control method takes advantage of the same environmental conditions as the eddy current solution by creating an intentional magnetic dipole on the satellite. In testing, 3U CubeSats show the ability to maintain ±15° pointing accuracy with respect to the local magnetic field. [19] Like the eddy current solution, this method can only provide two axes of control.

3) Gravity-gradient probe. A gravity-gradient probe is a dense weight placed on the end of a (relatively) long boom that deploys from the satellite after release from the launch vehicle. The boom must be long enough, and the mass heavy enough, to change the moment of inertia about the principal axis. Simply deploying the boom causes the satellite to naturally align the principal axis with the local Earth vertical and provides two axes of stabilization with approximately ±5° of pointing

accuracy about those two axes. [16] As can be seen from the example case, this method of control can produce considerable amounts of torque to provide two-axis stabilization. (FalconSAT-3, a USAFA "small sat," implements a gravity-gradient boom as part of its ADCS design.)

Chapter 3: Imaging Theory

Diffraction-Limited Performance

The performance of all imaging systems, both natural and manmade, is limited by diffraction. This theoretical upper limit is known as the diffraction limit and an optics system whose resolving power (ability to distinguish between two juxtaposed objects or points of light of slightly different wavelength) approaches meeting this theoretical maximum resolution is said to be diffraction limited. The closer two objects are to each other, the harder they become to resolve. If two objects are closer together than the diffraction limit, it is physically impossible to resolve the two objects. [20]

The accepted measure of the diffraction limit is known as the Rayleigh Criterion, which states: "two images are regarded as just resolved when the principal maximum of one coincides with the first minimum of the other." [20] This criterion is illustrated in Figure 9. The maximum theoretical angular resolution (the Rayleigh Criterion) of a round optic can be calculated using Equation 3.
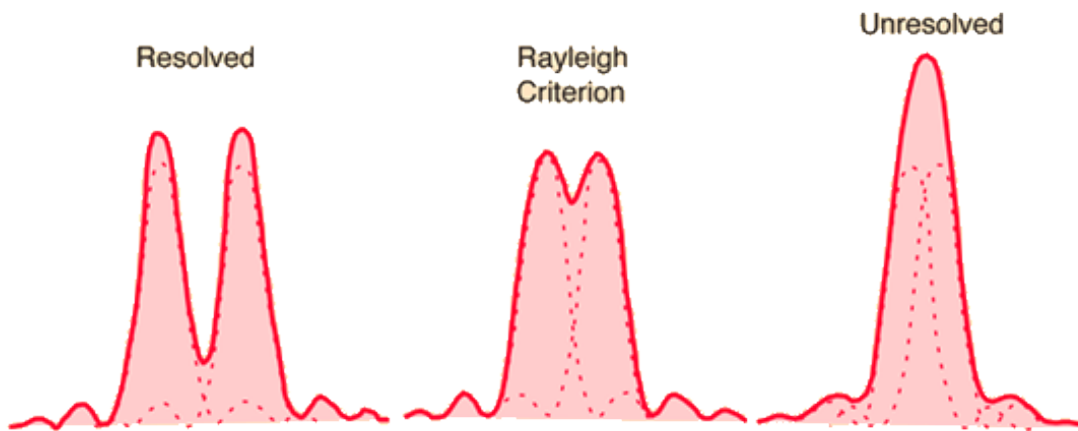
Figure 9: Illustration of the Rayleigh Criterion of Resolving Power [21]

Atmospheric Effects

For Earth-based optics attempting to observe objects through the atmosphere, it is all but impossible for the system's resolving power to approach the diffraction limit. The reason for this discrepancy is that the Rayleigh Criterion does not account for movement, vibration, poor manufacturing of the optic itself, or, most importantly (and hardest to account for), turbulent atmosphere. Changes in the refraction index of the air in the

different layers of atmosphere caused by non-homogeneous temperature, pressure, and humidity cause turbulence. [22]

The ability of an optic to "see" through turbulence in the atmosphere is very important. For some telescopes, this ability is limited by a parameter known as the Fried parameter (also known as coherence length). The Fried parameter is "a measure of the aperture over which there is approximately one radian of RMS phase aberration." The Fried parameter is denoted by r_0 and can be calculated using

$$r_0 = 0.185\lambda^{6/5}\cos^{3/5}(\zeta)[\int C_n^2(h)dh]^{-3/5}, \tag{11}$$

where λ is the wavelength being observed, ζ is the zenith angle (defined such that it equals zero at zenith and 90 degrees at the horizon), h is the height above the optic, and C_n is the refractive index structure constant, which is a parameter related to atmospheric turbulence. (In practical applications, the Fried parameter is measured rather than calculated.) [22] The Fried parameter can be approximately calculated using

$$r_o \approx \lambda^{6/5}. \tag{12}$$

However, for the visible spectrum, the Fried parameter typically has a value between 10 and 20 cm for ground-based optical systems (subject, of course, to the telescope location's time of day, weather, etc.). The resolving power of an optic can be approximated using the inverse of the Fried parameter (similar to Equation 3 except with the Fried parameter in place of the optic diameter), i.e., [22]

$$\theta \approx 1.22\frac{\lambda}{r_0}. \tag{13}$$

If r_0 is larger than the diameter of the primary optic, D, then the performance of the optical system will be limited by the diffraction limit. However, if r_0 is smaller than D, then the performance will be limited by the Fried parameter. The implication of this phenomenon is that, for a given observation location, increases in the size of the primary optic—beyond the size of the calculated Fried parameter—will have a very limited effect on the optical performance of the system (i.e., there is no benefit to manufacturing an optic larger than the Fried parameter. [22] Visually, this effect can be seen in Figure 10. As the normalized optic diameter (D_0/r_0) approaches and passes unity, the change in normalized resolution ($R/R_{\max}$) levels off. [23] Adaptive optics can be used to correct

some of the distortion caused by turbulent atmosphere, but even with adaptive optics, the effect of the atmosphere cannot be entirely undone.
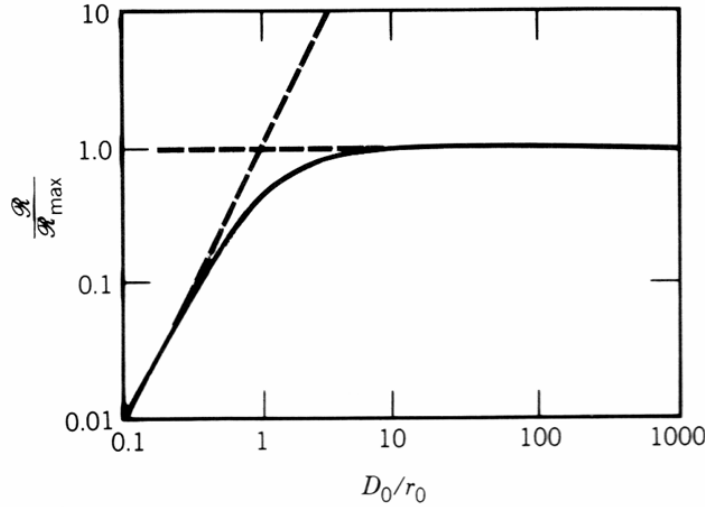
Figure 10: Effect of Normalized Diameter on Normalized Resolution for Long Exposure

Imaging Goal of the Falcon Telescope Network

The FTN consists of 13 sites all over the world (the 12 listed previously as well as USAFA). With the exception of the Air Force Academy in Colorado Springs, each telescope's primary optic is 20-in in diameter (the telescope at USAFA is 16 in). With a telescope so small, and over the large distances being observed, all of the images will be unresolved. With such a small and inexpensive telescope, there is little to nothing that adaptive optics can do to aid in image resolution. Some corrections are possible, however. Some aperture photometry corrections can be made such as error mass correction and normalization to a standard range (absolute magnitude). [24]

In testing, the 16-in telescope at USAFA was capable of detecting a 1U CubeSat, with no binning, in five seconds. Using two-by-two binning cuts the exposure time in half, but 2.5 sec is still a long exposure time. In some cases, the right solar phase angle allowed a shorter exposure time. From USAFA, most 1U CubeSats observed fell in the 12–15th absolute magnitude [24] (1.84 W/m^2 to 1.16×10^{-1} W/m^2 luminosity) range [25].

Such a long exposure time guarantees an unresolved image because atmospheric effects are detrimental enough to fast shutter speeds, let alone long exposures. With long shutter times, there are an even greater number of possible effects to take into account. The goal resolution for each site is about 2 arcsec (9.70 μrad). The ideal resolution, at 550 nm, is 0.27 arcsec (1.32 μrad), but that figure is impossible to obtain. For example, at the Air Force Academy, in near perfect observing conditions it is possible to achieve about 1.3–1.5 arcsec (6.30–7.27 μrad) resolution. Being at 7,280 ft above sea level, telescopes at USAFA have substantially less atmosphere to see through and, even in this improved observing condition, USAFA's telescope still cannot approach the calculated ideal. The goal, then, for the FTN is to determine how much can be learned about an object from the optical signature of the unresolved image or images. It may also be possible, and interesting, to observe the same target simultaneously from various lightings and see what, if any, information can be gleaned from the comparison of those images. [24]

Target Detection

One important consideration to take into account is how large the target needs to be in order to be above the detection threshold of the FTN telescopes. The problem setup can be seen in Figure 11. The solar flux that reflects off the target satellite (at the surface of the satellite) can be calculated using

$$F_R = 1240 \times A \cos(\theta_i) \cos(\theta_r) \,. \tag{15}$$

After the light from the Sun reflects off the target satellite, the flux must then propagate through Earth's atmosphere to the telescope. The flux that theoretically reaches Earth's surface is calculated using (assuming a Lambertian reflection surface and no extinction through the atmosphere)

$$F_G = \frac{F_R}{2\pi r^2} \,, \tag{16}$$

where r is the distance between the satellite and the telescope in meters. The best case scenario for maximum reception of the Sun's reflected light was for the telescope to be near dawn or dusk and for the satellite to be on the line created by the sun and the edge of Earth (see Figure 12).
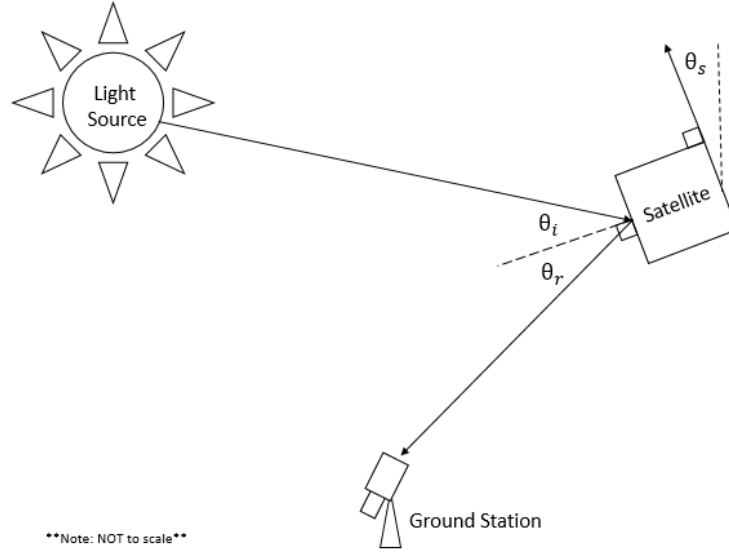
Figure 11: Solar Flux Reflection Problem Setup
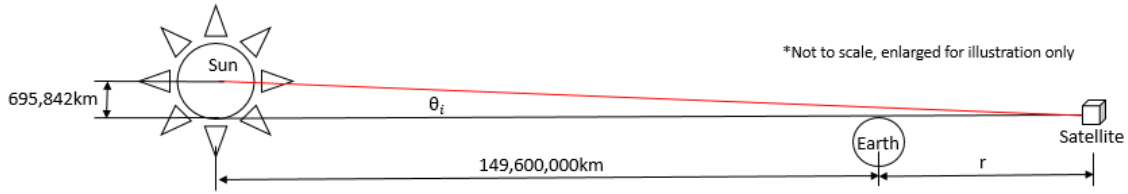
Figure 12: Illustration of Best Case Reflection Scenario

In this scenario, the smallest (and best) angle of incidence onto the satellite is 0.265°. The telescope should be as near as possible to dawn or dusk while still allowing observation of the satellite. Ideally, the reflected angle should be zero degrees, but in reality this is not possible. For the purposes of analysis, it is assumed that the reflected angle is equal to the incident angle to maximize the light reflected. This calculated value for maximum reflected light received is the threshold that was used to determine if the FTN could detect various size targets.

Before selecting the target size, it is important to determine how small a target the FTN is capable of detecting. The specifications for the camera (given in Table 2) indicate that the CCD has system noise of 15 electrons at 1 MHz. In other words, exposed to absolutely zero light, the CCD would "detect" 15 photons per pixel per microsecond. In order for a target to be visible, it must be brighter than this system noise. The flux at the ground, F_G, could be used to calculate if a target of that intensity is detectable using

28

$$P = \frac{F_G A_l (\text{Q.E.})(\text{optical thruput})}{E_{\text{photon}}}. \qquad (17)$$

In this equation, A_l is the area of the telescope lens, Q. E. is the quantum efficiency of the CCD (whose exact values at various wavelengths can be found in Figure 2), optical throughput is essentially the efficiency of the entire system (there will be some loss at every lens and thus significant loss throughout the system, for this calculation, it was assumed to be 0.5), and E_{photon} is the amount of energy in a single photon of a particular wavelength. E_{photon} can be calculated using

$$E_{\text{photon}} = \frac{hc}{\lambda} = hv , \qquad (18)$$

where h is Plank's constant (6.63×10^{-34} kg·m^2/s), c is the speed of light in a vacuum, λ is the wavelength of the photon of interest, and v is the frequency of the photon of interest. Once the value for P (number of photons detected per pixel per microsecond) is calculated, it is compared to the CCD specification. [23] In order to be detectable, P must be greater than 15.

As for CubeSats, the sizes of greatest interest to the FTN program would be the 1U and the 27U sizes, because of their symmetry. Conducting the above calculations for these two sizes, it is found that at 550 nm, the 1U CubeSat (under perfect reflection and observation site conditions), with a Lambertian surface, was only marginally detectable in a 200-km orbit with only about 13 photons per pixel per microsecond detected, just below the noise threshold. In an orbit higher than 200 km, the flux from the reflection off a 1U CubeSat dies off too quickly before reaching the detector. Additionally, at this low altitude, the CubeSat has a lifetime less than one month. The 27U CubeSat, however, is found to be detectable at all wavelengths in the visible spectrum, at all altitudes of interest to this program (200 to 450 km). Even at 450 km, the 27U CubeSat (under the assumed nearly perfect conditions) has a detection rate of 31 photons per pixel per microsecond, well above the noise level. The flexibility of orbital altitude and easier detection provided by a larger target proves to be critical in the selection phase of the target.

At first glance, the calculations may seem to be conflicting with the experimental results from the USAFA 16-in telescope. However, as mentioned before, the USAFA observatory is at a great advantage because there is less atmosphere to disturb the images.

Additionally, the rough calculations conducted here assume Lambertian reflection. Most of the 1U CubeSats in orbit have at least some specular reflection due to their solar panels and aluminum construction. Having specular reflection significantly decreases the exposure time needed to detect a target. Dr. Francis Chun at USAFA believes that, in general, the FTN telescope sites should be able to detect objects down to about 16th absolute magnitude (4.63×10^{-2} W/m^2 luminosity) [25]. At USAFA, he hopes to obtain detections down to about 20th absolute magnitude [24] (1.16×10^{-3} W/m^2 luminosity) [25].

Chapter 4: Design Proposals

There were a number of ways to approach the design of an appropriate target for optical calibration of the FTN. The choice of target design was a function of cost, mission effectiveness, ease of construction, and required personnel hours to construct and operate post-launch. Some possible options included:

1) <u>A "dumb" target</u>. These targets are purely passive; they have no attitude control or communication and do not change in any way in orbit. These targets are on the low end of the cost and personnel hour spectrum.

2) <u>A passively changing satellite</u>. These targets do not have communications systems but do change in a predictable and/or known way once in orbit. There are a number of parameters that could be changed in orbit without requiring communication with the satellite. The space environment can trigger changes in parameters in a number of ways, including atomic oxygen exposure, temperature change, and light exposure. Each of these triggers provides a unique capability to change the dynamics of the satellite in a predictable manner without having to communicate with it.

3) <u>A passively controlled satellite</u>. Environmental factors such as Earth's magnetic field, the passage between sunlight and eclipse, as well as orbital mechanical factors, allow for control methods that do not require communication with the satellite to execute them. These are less expensive than active control methods and do not require personnel hours after launch. These control methods can generally maintain attitude within about $\pm10°$ of a specific axis, be it Earth's local magnetic field or the local Earth vertical.

4) <u>An actively controlled satellite</u>. These satellites are at the high end of the cost and personnel hour spectrum. Not only do they contain all the typical subsystems (Attitude Dynamics and Control Systems, communications, etc.), but they also require ground station monitoring and communication in order to obtain attitude data and control the attitude of the target as desired. The subsystems can be as simple or as complicated and/or numerous as necessary to meet the mission requirements.

Each design option has its own advantages and disadvantages so the choice of target depends entirely on the priorities of the user. Each are discussed in more detail below.

"Dumb" Targets

A "dumb" target is one that does not require any attention post-launch and has no way of changing parameters in orbit. These targets are comparatively inexpensive, to the point of "disposability" (capable of being produced *en masse* with little to no concern over the loss of one or more units), and can be launched in clusters to increase effectiveness. A "dumb" target for the FTN could consist of "painting" each side of the CubeSat with a unique and known color, for example: full reflect, full absorb, low spectrum (blue) reflection, and high spectrum (red) reflection. These four colors can be strategically divided among the six sides of the cube such that any viewing angle on the satellite will produce a unique color combination that will allow for attitude determination.

A similar program, called Occulus-ASR, is a satellite designed by the Michigan Technological University with the goal of providing calibration and validation for the Air Force Maui Optical Station's telescopic non-resolved object characterization program. [26] In this way, the Occulus-ASR program has a goal that is very similar to the FTN calibration target. Occulus-ASR uses a color scheme of white, red, yellow, and blue, but in their analysis, the Occulus-ASR team suggests that white, red, green, and blue might provide better optical contrast. If this design solution is the desired route for the FTN, it would be wise to take this recommendation into consideration. It would also be wise to consider using common space materials on each of the panels (each with a different optical signature) since the ultimate goal of the FTN is to translate information learned about the calibration target to operational, unknown targets. Another recommendation that the Michigan Tech team makes is to use more diffuse, rather than specular materials, to increase signal strength at non-specular angles. However, it may be possible to find a way to utilize both diffuse and specular materials.

An addition that could be made to this "dumb" design is to place fused silica glass retro reflectors on each of the eight corners of the cube. These retro reflectors are highly

reflective and will produce a very bright signature that will appear brighter on the ground than the rest of the satellite. In order for these retro reflectors to be effective, however, the FTN sites would have to be equipped with the equipment to actively illuminate the targets, i.e., with a laser. These bright spots allow for calculations of spin rate and other useful knowledge that would be more difficult to glean from the unique color scheme alone. This addition is similar to the PERCS satellite discussed in Chapter 2.

Passively Changing Targets

Passively changing targets are the midpoint of the cost and personnel hour spectrum. These targets change their color or shape in orbit due to interaction with the environment (i.e., atomic oxygen or radiation exposure), or they change their attitude as a result of interaction with Earth's magnetic field or changes in temperature and/or light due to passage through Earth's shadow. The advantage to using passive change is that it exhibits a way of taking advantage of environmental factors that are present no matter what, and which are generally considered disadvantages.

The first passive change trigger discussed is atomic oxygen. Atomic oxygen typically has a detrimental effect on satellites, but it is possible to utilize its presence as an advantage. Atomic oxygen can affect a satellite in three different ways:

1) Atomic oxygen degradation. Using a material that degrades in the presence of atomic oxygen allows the entire satellite to change shape in some way by using a degrading trigger or switch to activate a dynamic change once the trigger degrades sufficiently. Possible options for shape change include, but are not limited to: a mechanism for turning the cube into a sphere or another shape, or "deploying" one or more panels. Table 8 summarizes sample polymers that show both high and low degradation (erosion yield) in the presence of atomic oxygen on the MISSE 2 PEACE test onboard the International Space Station (ISS).

2) Atomic oxygen ablation. Some materials, such as cellulose acetate, degrade and flake off in the presence of atomic oxygen. Placing a thin layer of this material over another base material that does not degrade would make the target change color and, thus, reflectivity, in orbit. Alternatively, a thin strip of this material can be used to create a trigger mechanism that can cause a dynamic change. See Table

8 for examples of materials on the MISSE 2 PEACE test that show high ablation (structural change).

3) <u>Atomic oxygen color change</u>. Atomic oxygen exposure changes the color of some materials. Kapton H, for instance, changes from black to orange in the presence of atomic oxygen. (Unfortunately this process is somewhat slow; a different material choice may be beneficial. See Table 9 for more details.) This method is, perhaps, the simplest passive change mechanism. Table 9 includes a sample of notable color changes, or lack thereof, for the MISSE 2 PEACE test.

Although not explicitly explored, exposure to radiation (UV or cosmic) might also provide changes in material properties that could be exploited.

Table 8: MISSE 2 Atomic Oxygen Exposure Results of Materials with Greatest and Least Mass Loss Over 3.95 Years Exposure to 8.43×10^{21} atoms/cm^2 AO Fluence [27]

Material Name	Mass Loss (g)	Erosion Yield (cm³/atom)	Structure Change	MISSE S/N
Polyoxymethylene (POM)	0.37838	9.14×10^{-24}	N/A	2-E5-12
Allyl Diglycol Carbonate (ADC)	0.26730	$>6.80 \times 10^{-24}$	Peeling	2-E5-14
Polymethyl Methacrylate (PMMA)	0.19459	$>5.60 \times 10^{-24}$	Peeling	2-E5-16
Cellulose Acetate (CA)	0.19148	5.05×10^{-24}	Peeling	2-E5-7
Polyimide – Kapton H (PI)	0.12478	3.00×10^{-24}	N/A	2-E5-30
Fluorinated Ethylene Propylene (FEP)	0.01248	2.00×10^{-25}	N/A	2-E5-42
Amorphous Fluoropolymer (AF)	0.01235	1.98×10^{-25}	N/A	2-E5-45
Perfluoroalkoxy Copolymer Resin (PFA)	0.01079	1.73×10^{-25}	Dimpled	2-E5-44
Polytetrafluoroethylene (PTFE)	0.00894	1.42×10^{-25}	N/A	2-E5-43
Crystalline Polyvinylfluoride with White Pigment (PVF)	0.00471	1.01×10^{-25}	N/A	2-E5-11

Note: Erosion yields listed with a > symbol indicate polymers that were eroded partially or completely through all layers.

Should a stable color scheme be desired, it will be important to choose materials that maintain their color in the space environment. Some of these materials are listed at the bottom of Table 9. Because of its stability in both appearance and structure, gold foil is a very common satellite coating. Gold foil remains gold in color and shiny when exposed to atomic oxygen, and it does not ablate or degrade in the presence of atomic oxygen.

Alternatively, a non-stable material can be used and coated with a thin protective layer that is stable in the space environment. One possible option for a space protective coating is a new material called a ceramer (a ceramic, polymer compound) developed at the University of Akron. The material is a hybrid of silicone/siloxane (combining organic and inorganic material) that is optically transparent and "can offer protection from atomic oxygen as well as UV radiation and high-energy particles via the in situ fabrication of nanophase silicon/metal-oxo clusters." [28] These silicon-oxo clusters offer protection from UV-radiation at the 290–400 nm wavelength, which helps prevent "yellowing" of the underlying material.

Table 9: MISSE 2 Atomic Oxygen Exposure Results of Materials with Notable Color Change Over 3.95 Years Exposure to 8.43×10^{21} atoms/cm^2 AO Fluence [27]

Material Name	Color Change	MISSE S/N
Epoxide (EP)	Tan to Salmon	2-E5-19
Polyimide (Kapton H)	Black to Orange	2-E5-30
Polyimide (Kapton HN)	Black to Burnt Orange	2-E5-31
Polyimide (Upilex-S)	Black to Tan Gray	2-E5-32
High Temperature Polyimide Resin (PMR-15)	Black to Dark Red	2-E5-34
Crystalline Polyvinylfluoride With White Pigment (PVF)	N/A (White)	2-E5-11
Polyoxymethylene (POM)	N/A (Light Gray)	2-E5-12
Polybutylene Terephthalate (PBT)	N/A (White)	2-E5-21
Pyrolytic Graphite (PG)	N/A (Black)	2-E5-25

In testing, the ceramer hybrid coating, exposed to moderate AO fluence (up to 2.22×10^{21} atoms/cm^2), shows low mass loss of the underlying material and shows no evidence of microcracking in the coating. The absence of microcracking means superior specular light transmittance. Unfortunately, at high fluence (up to 1.38×10^{22} atoms/cm^2) the material fails. The AO fluence experienced by the polymers on MISSE is just over half way between the testing levels of "moderate" and "high" fluence for the ceramer. Therefore, the performance of the material in the LEO environment would likely be worse than the "moderate" fluence level testing results but not as bad as the "high" fluence level results. For this reason, and for the purpose of reducing exposure to the harsh space environment in general, it would be best to choose an orbit with a higher altitude. When the stability of the color of the underlying material is of high interest, new protective coating materials, like this one, could prove to be useful in avoiding having to find or create a space stable material with the desired optical properties.

Passively Controlled Targets

In addition to passively changing targets (targets whose properties change without command), passively controlled targets are also an option. Passively controlled targets are capable of maintaining some degree of attitude control without requiring command. Some of these passive control options include:

1) Interaction with Earth's magnetic field. It is basic physics that conducting components traveling at high speed through magnetic fields will induce eddy currents. If the satellite is symmetrical then the forces created by these currents will cancel out. However, if the satellite is made intentionally asymmetrical it could theoretically be possible to utilize the net force created in a favorable and predictable way. This effect can be achieved with either a PMAC system or an eddy current design, as discussed previously.

2) Light interaction. The passage of the satellite through Earth's shadow at a regular period changes the light exposure, and thus the temperature, of the satellite. Knowing this, one could utilize some form of photoresistor to induce changes in

36

the dynamics of the satellite or a thermal conduction of some kind (such as a
bimetal switch or expansion to create a circuit) to induce a desired change.

3) <u>Gravity-gradient boom</u>. The satellite can be programmed such that after a certain
amount of sun exposure a gravity-gradient boom is deployed. Once the boom is
deployed, no commands are necessary but two-axis stabilization is still present.

It is also possible to design a target that uses multiple passive ADCS methods for better
accuracy. Each of these solutions presents a different method of exploiting the naturally
occurring phenomena in the space environment and attempting to turn common
disadvantages into advantages without greatly increasing cost of construction or post-
launch personnel hours.

Actively Controlled Targets

Actively controlled targets are the most expensive solution and the only solution
that requires post-launch personnel hours in a ground satellite operations center. A simple
case of active control is to move the solar panels to change the aerodynamics of the
satellite. This doesn't necessarily have to be an active control system; it could be
programmed to change position of the panels at regular intervals or in response to light or
temperature, as previously discussed. However, it can be done as an active control, too.

The more complex solution is to incorporate all the usual subsystems into the
satellite. This solution is the most costly option because these subsystems are expensive
in and of themselves. However, it also requires a ground station—which is costly—and
personnel hours to download and compare the attitude data to the observed data from the
telescopes. (While all target designs will require analysis of the telescope data, an
actively controlled target has the unique addition of comparison to known attitude which
will require extra work.) This solution has the advantage of knowing the exact attitude of
the satellite at any site where it is being observed so that the observed image can be
compared to the known attitude.

Chapter 5: Design Proposal Comparison and Selection

Design Comparison

To this point, a number of possible solutions for a calibration target design for the FTN have been discussed. However, many of these solutions are either impractical, do not have flight history, or are poor choices for other reasons. Each of the design options was discussed briefly in preceding chapters with enough detail to begin to rule out design proposals. Based on the solar luminosity predicted to be received on the ground from reflection off the target, a 27U CubeSat is the preferable choice for target size over the 1U CubeSat. A summary of the relative cost, complexity, and post-launch personnel hours for each of the designs discussed can be found in Table 10.

1) <u>Unique color scheme</u>. From a cost perspective, this choice is the lowest cost in terms of both design/production and personnel hours. However, this type of design, when deployed, would tumble freely in space. Because of the small size and low moment of inertia, the spin rate has the potential to be fairly high. With the low optical resolution of the telescopes, it will be difficult to an accurate optical signature with enough detail to make a good determination of information about the satellite.

2) <u>Unique color scheme and retroreflectors</u>. The reasons to not use this design are mostly the same as those discussed above for a target with only a unique color scheme. However, with this design, there is the additional requirement to retrofit some or all of the telescope sites with an active illumination source, such as a laser. In addition to the time needed to make these changes, adding lasers to the sites would also significantly increase the cost of each telescope unit.

3) <u>Atomic oxygen ablation</u>. A 27U CubeSat in a 350-km circular orbit has a predicted lifetime of 2.7 years, which, based on MISSE, is enough time for some materials to begin to ablate due to atomic oxygen exposure. However, the downside of basing a design off of the results of MISSE is that MISSE II was 3.95 years long and in that exposure time, there were no mid-exposure measurements or data recorded. As a result, there is not a clear understanding of the timeline under which these changes occur. In order for the satellite to be in

orbit long enough to have enough exposure to atomic oxygen to ablate, a 27U CubeSat would have to be above the altitude of the ISS where the MISSE data were collected. As altitude increases, the density of atomic oxygen decreases, meaning that the higher the altitude of the satellite, the longer it will take for the ablation to occur. The unpredictability of the behavior of the material for this method makes it less than desirable as a calibration strategy.

4) <u>Atomic oxygen color change</u>. As with the atomic oxygen ablation design above, the unpredictable nature of this design makes it undesirable as a calibration target.

5) <u>Atomic oxygen degradation</u>. Again, many of the same reasons discussed above made this design undesirable. However, these designs (both degradation to change shape and degradation to move the panels) involve the added uncertainty and complexity of designing a dynamic system that will change based on an unpredictable trigger. However, this design has the benefit of changing in a more predictable way than other designs. Once the trigger is activated, the change in the satellite is well known/understood. Unfortunately, there is a great deal of complex design involved in creating an AO degrading trigger and dynamic system. Practically, the excess work and the unknown of the triggering device are not worth the small added benefit of knowing how the target would change. Additionally, even though the second stage shape is known, the time it would take to get to the second stage is not.

6) <u>Eddy current interaction</u>. In terms of magnitude, the force created by magnetic field interaction is in the mid-range of solar radiation pressure, magnetic field interaction, and atmospheric drag. Eddy currents are a well-documented force on satellites in orbit and have been studied since the conception of space flight. However, the majority of this investigation has been with the goal of limiting or dampening the effects of eddy currents, not in taking advantage of eddy currents as a way of controlling the satellite. This design proposal, therefore, has no flight history or test data to determine if it would, in fact, be effective in space flight. More research will need to be conducted into eddy current control before this proposal would be viable.

7) <u>PMAC</u>. Another form of magnetic field interaction, the magnitude of this force is predicted to be mid-range of the four main perturbations discussed. PMAC is in the proposal stages itself and has been simulated and shown to be fairly effective at maintaining the attitude of the satellite. However, as with the eddy current proposal, this design does not have flight history and should be tested further before an attempt is made to implement it in a calibration target.

8) <u>Gravity-gradient boom</u>. Of the four main perturbations discussed, gravity-gradient has the greatest magnitude, by far. Gravity-gradient booms have a long flight history and are well documented and understood. Of the dynamic design options proposed, this design is the simplest because it only has to move once, rather than repeatedly. The amount of movement, and the complexity of the design required, are less than the other designs. By placing a solar panel on the side opposite that from which the boom deploys, as well as around the hole the boom deploys from, the satellite can be programmed to deploy the boom once a battery has charged to a certain point. Once the boom has been deployed, the boom will constantly point toward, or away from, Earth (providing two-axis stabilization) and the adjacent four sides will be visible to the ground from various angles. This is the first of the truly viable design options.

9) <u>Photoresist</u>. Using a photoresistor as a switch for a dynamic system has its own complexities. A photoresistor switch could make it so that the satellite would have one shape when exposed to sunlight and another shape when in Earth's shadow. In order to detect the reflection from a target, the telescope would have to be in the dark and the satellite would have to be in the light. Therefore, the satellite would only be viewable in one of the two modes and the other would be mostly wasted. Alternatively, the switch could be programmed so that the mode changes each time the satellite reenters the sunlight. In this way, every other time the satellite is visible to a given telescope the shape would be different. This design requires significant power and a fairly complex design including numerous actuators to execute the shape changes. Depending on which shape change was actuated, the satellite may or may not have pointing stability. As discussed previously, lack of pointing stability for such a small target will be largely

detrimental. The added complexity and cost of this design is not worth the minimal advantage potentially gained by changing the shape of the target.

10) <u>Bimetal</u>. A bimetal switch works much the same as the photoresistor switch. When the satellite is in the sunlight, it heats up and the bimetal switch bends to complete a circuit that would cause the satellite to change shape. When the satellite cools off, the switch bends back and opens the circuit. Again, the satellite can be programmed so that each time the circuit is closed, it switches modes (i.e., enters mode number one when entering the sun and remains in that mode in Earth's shadow, enters mode number two when re-entering the sunlight and remains in that mode, and then returns to mode one when entering the sun once again). As with previous designs, this design also lacks pointing stability. Again, the added complexity of this design, for little intellectual gain, make it an inappropriate choice for an initial calibration target choice.

11) <u>Full ADCS</u>. This is by far the most expensive option. CubeSats are definitely less expensive than "small sats", which have at least 20 times more volume, but a full set of subsystems for a CubeSat is not inexpensive by any means. It is entirely possible that the full cost to design and build a fully active 27U CubeSat could exceed the cost of all of the telescopes combined (about $2 million). Because of the excessive cost of this design, it is not a desirable first round choice, but it could potentially be implemented in future design revisions should the initial designs be successful. The major advantage of this design is that the user can command dynamic changes if desired. If not, the user could at least receive exact data about attitude to compare to what is imaged on the ground. In the end, attitude data will prove to be most useful in backing out exactly how much can be gleaned about a target based on the unresolved images.

Table 10: Comparison of Possible Target Designs

Design Method		Design	Relative Cost	Design Complexity	Post-launch Personnel Hours
"Dumb" Target		Color Scheme	Low	Low	None
		Color Scheme with Retroreflectors	Moderate	Low	None
Passive Change	AO Ablation	Change Color	Low	Low	None
	AO Color Change	Change Color	Low	Low	None
	AO Degradation	Change Shape	Moderate	High	None
		Move Panels	Moderate	High	None
Passive Control	Magnetic Field Interaction	Eddy Current	Moderate	Moderate	None
		PMAC	Moderate	Moderate	None
	Gravity-gradient	Boom	Moderate	Moderate	None
	Light Interaction	Photoresist	Moderate	High	None
		Bimetal	Moderate	High	None
Active Control		Full ADCS	High	High	Routine Operation

Design Selection: Gravity-Gradient Boom

Based on the comparison detailed above, a target with a gravity-gradient boom is viewed as the best initial target design for the FTN. The gravity-gradient boom has been used for passive control of satellites for decades. It is a fairly simple design concept; after deployment from the P-POD, the CubeSat will be in free tumble. Without a command to do so (which would require a communication subsystem), the satellite will deploy a collapsible boom that is stored inside the CubeSat during launch. The boom should be at least a meter long with a small, dense weight on the end away from the satellite. Deploying the boom shifts the moment of inertia of the satellite and causes it to stabilize in a position with the boom constantly pointing toward, or away from, Earth. It is possible, depending on the attitude at the time that the boom is deployed, for the stable deployed configuration to be with the satellite closer to Earth and the boom weight pointed away from Earth.

Regardless of whether the satellite or the boom mass is closest to Earth, the sides adjacent (perpendicular to the surface of Earth) are the sides that would have the unique colors on them. Depending on the spin of the satellite about the boom axis, and the location of the telescope with respect to the satellite, one or more of these unique sides will be facing the telescope at any given time.

Since the mission of the FTN is eventually to determine information about unknown targets, it is best to make the sides of the target from materials that are both common on the outside of spacecraft and have unique optical signatures. For this reason, it makes sense to utilize pyrolytic graphite, aluminized Kapton film, gold foil, and polished aluminum. The gold and Kapton sides should oppose each other since these sides have the most similar optical signature. However, as the Kapton is exposed to atomic oxygen it will blacken, causing two adjacent sides to appear black in color. (Even though they both appear black in color, the reflectance properties of the two materials are different, see Figures 14 and 15.) Solar panels are placed on the boom deployment side and the opposite side, serving the dual purpose of providing power for the boom deployment as well as a fifth, unique optical signature. Using these materials on the calibration target allow inferences to be made about how the same materials behave on other objects of interest in orbit.

The boom is deployed after the solar panels cause the satellite to collect enough battery charge to deploy the boom. The solar panels provided enough power to drive an actuator to deploy the boom once, after the boom deploys, the solar panels are no longer necessary. In the worst case scenario when the boom fails to deploy for some reason, the solar panel sides will not be wasted because they will still provide an optical signature that is differentiable from the other sides; the target simply becomes the first design proposal of a free tumbling satellite with a unique color scheme.

Material Properties

It is critical that, once in orbit, each side of the target is distinguishable. However, with the low resolution of the FTN telescopes and the small size of the target satellite, the "images" of the target will likely not be resolved enough to actually visually distinguish between the various colors. Instead, color differentiation will have to be in the form of detecting differences in the intensity of reflected sunlight detected. The amount of sunlight reflected off the satellite and down to the telescope depends on the reflectivity of each material. The special materials selected, in order of decreasing reflectivity, are: aluminum, gold foil, aluminized Kapton film, and pyrolytic graphite. Solar panels, which are also discussed, are less efficient reflectors than aluminized Kapton film but more

efficient than pyrolytic graphite. The reflectance of aluminum and gold over various wavelengths can be found in Figure 13.

In orbit, both the gold foil and the aluminum will be stable both in color and structure. However, the aluminized Kapton film will slowly blacken over time and become increasingly matte. Even before atomic oxygen exposure, the Kapton film is not a highly efficient specular reflector, but as the film blackens it becomes ever less specularly reflective. A comparison of specular and diffuse reflection of pre- and post-atomic-oxygen-exposed aluminized Kapton film can be found in Figure 14. It is important to note that, before atomic oxygen exposure (at the beginning of the mission), the aluminized Kapton has a diffuse reflection of zero over the visible spectrum and, as the mission continues, the diffuse reflective efficiency of the aluminized Kapton increases to as much as 25% in the mid-range of the visible spectrum. At the same time, the specular reflection in the mid-range of the visible spectrum decreases from about 40% to about 5%. This is a unique quality of the aluminized Kapton film that should be observable by the FTN.
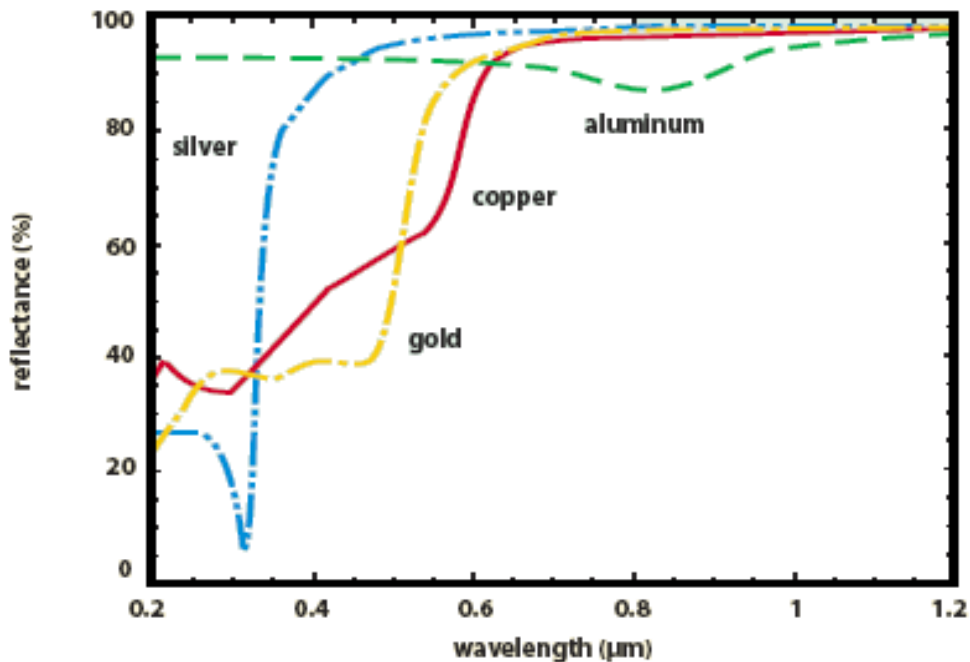

Figure 13: Reflectance of Various Shiny Metals over Various Wavelengths [29]
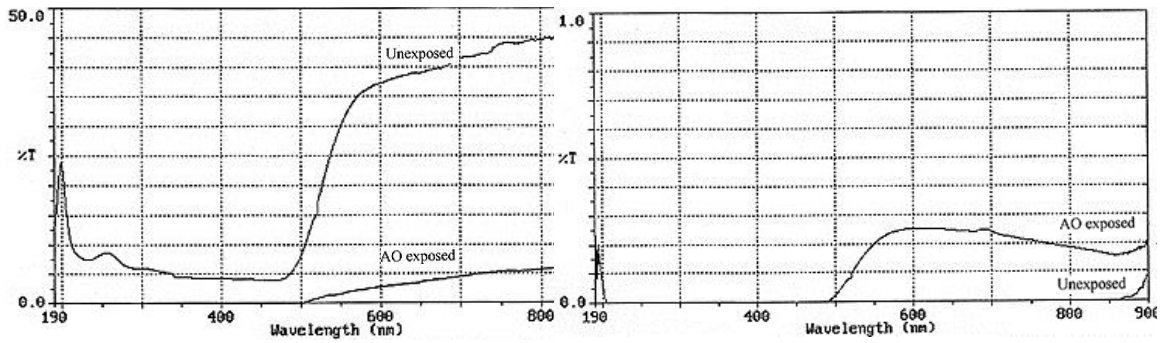
Figure 14: Specular, 90° (Left) and Diffuse, 45° (Right) Reflection from ¼ mil Aluminized Kapton Film [30]

The last special material for the lateral sides of the CubeSat was the pyrolytic graphite. In MISSE testing, over nearly four years of atomic oxygen exposure, pyrolytic graphite proved to be stably black in color without showing signs of structural damage. [27] The reflectance for pyrolytic graphite can be found in Figure 15. It is the least reflective of the materials chosen, which is to be expected for a black surface.
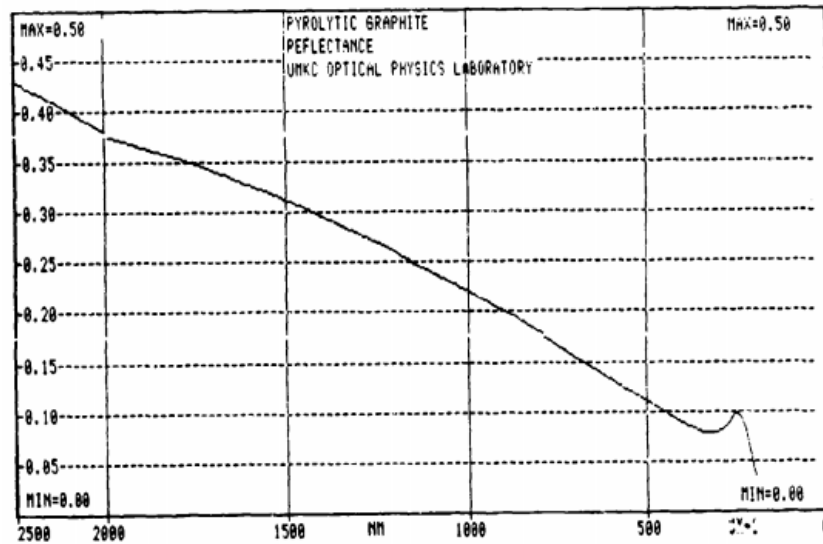

Figure 15: Reflectance Spectrum of Pyrolytic Graphite [31]

Finally, the solar panels necessary to provide power to deploy the boom are made of silicon under glass. The reflective properties of silicon can be seen in Figure 16. While it is common (for power purposes) to minimize reflection off the solar panel, for the purposes of this mission (limited required power and desired reflection) it is more detrimental than beneficial to use an anti-reflective coating.
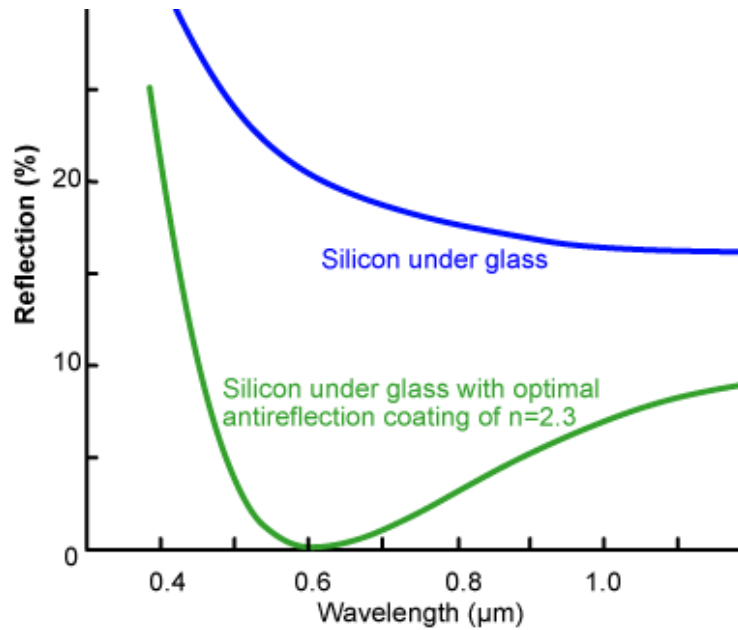
45

Figure 16: Comparison of Surface Reflection for a Silicon Solar Cell [32]

Design Considerations

Because of the way the target is designed, it is only visible to the telescope when the telescope is in the dark and the target is illuminated. The gravity-gradient boom of the satellite keeps the boom either constantly pointed toward or away from Earth. The colored calibration panels are, therefore, always perpendicular to the local surface of Earth and would rarely have the correct geometry for the Sun's rays to reflect off of the sides and down to Earth. Angling the side panels after deployment is one way to mitigate the poor reflection geometry issue.

When the boom deploys, the satellite will stabilize to the closest low energy pointing, which could be with the boom pointing toward or away from Earth. Which direction the satellite stabilizes in depends on the spacecraft attitude when the boom is deployed, which is affected by the launch vehicle, the P-POD deployment, and a number of other unpredictable influences. For this reason, it is nearly impossible to determine which direction to "unfold" the side panels. Instead, when the boom deploys, the same actuator is used to "flatten" the satellite, pushing the side panels out into a tent-like structure allowing for a much more appropriate reflection geometry, regardless of the attitude the satellite settled in. Figure 17 shows a model of the satellite before and after boom deployment.
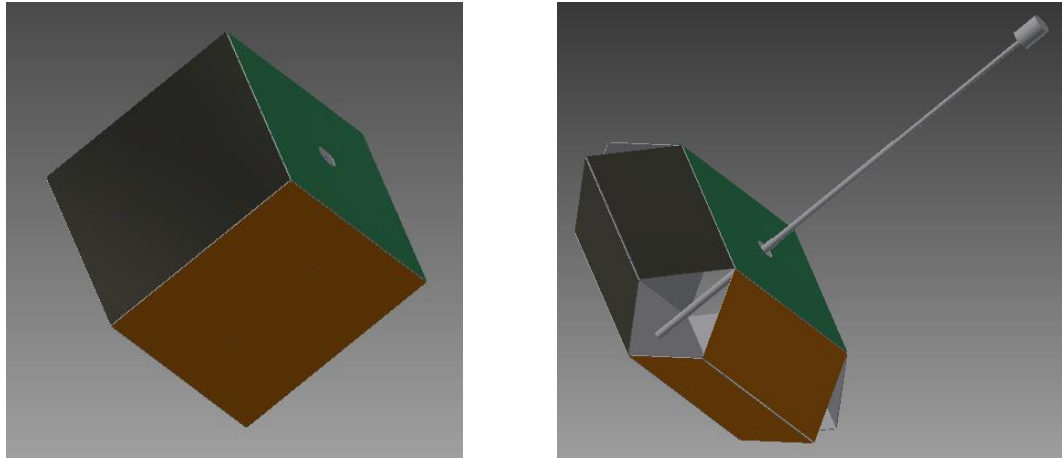
Figure 17: Model of Satellite Before (Left) and After (Right) Boom Deployment

Because of the viewing conditions required for the satellite to be visible, the target is only observable directly overhead from approximately 0330 to 0600 and again from 1800 to 2030 local time (times when the telescope is in the dark and the satellite is illuminated, see Figure 18). The angle to which the side panels of the target collapse (δ in Figure 19) is dependent on the time of day for which the angle is optimized. The farther away from the Sun the target is, the farther the side panels have to collapse in order to provide the most ideal reflection geometry.
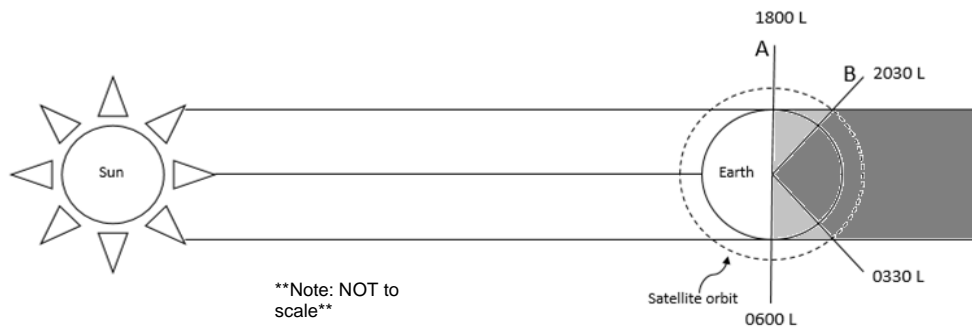

Figure 18: Local Observability Times for Target Satellite

As far as strength of reflected signal, the best times of the day are approximately 0330 and 2030 local time as these are the times when the angle of incidence of the Sun's rays have the potential to be the smallest. However, if the target is optimized for this angle, the reflection at every other time of the day will be fairly poor. The better design choice is to optimize the angle for a time somewhere between the start and the end of a

47

visibility window so that the signal starts weaker then gains strength before dimming once more. In the evening visibility window, the optimal angle, δ, is about 45° at 1800 (point A in Figure 18). The optimal angle at 2030 is about 25° (point B in Figure 18). Therefore, an angle of 35° optimized for approximately 1930 is used (see Figure 19). The optimal angles for the morning visibility window are the same (25° at 0330, 45° at 0600, and 35° at 0430). All times referenced herein are for observing a satellite directly overhead. (It is possible for a ground station to observe a satellite closer to the horizon at midnight—directly over a point on the ground that is experiencing an earlier time of the day—but for simplicity of calculations, only a point directly overhead is considered.)
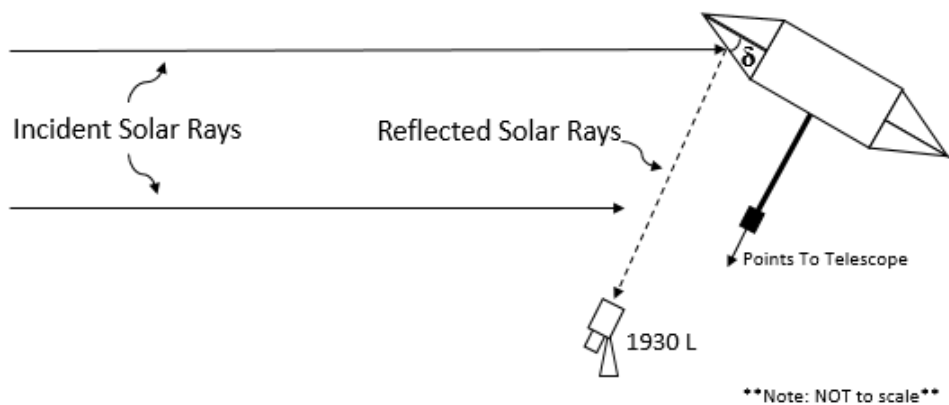

Figure 19: Panel Angle Design Choice for Evening Visibility Window

In addition to the fact that the target will be largely non-visible to the telescopes if the sides are not collapsed, this design has a number of other advantages as well:

1) The satellite will be equally visible and will absorb the same amount of power with the solar panels regardless of the orientation of the satellite after the boom is deployed and the satellite has stabilized.

2) Flattening out the satellite would increase the moment of inertia, which helps to dampen and/or resist any spin that the satellite would have about its boom axis.

3) Creating a sharp, rather than flat plate, surface in the direction of travel of the satellite makes it more aerodynamic and increases the stability of the spacecraft, which aids in maintaining the desired pointing stability.

The mechanics used to deploy the boom can be modified to flatten the satellite at the same time by using a worm gear or similar mechanism to pull the "top" and "bottom"

48

panels of the satellite closer to each other as the boom deployed. Doing so will not greatly complicate the design of the satellite, nor will it greatly increase cost.

Expected Signal

As stated before, the "image" will be so unresolved at the telescope that the spectral signal, more than the actual image, will be of importance. Therefore, it is important to estimate the spectral signal that will be received when viewing each side of the target. One way to calculate this estimate is to multiply the reflectivity curves presented above by the irradiance of the Sun that passes through Earth's atmosphere [33]. Doing so represents the greatest amount of irradiance that can be reflected off the satellite at each wavelength. Once that is determined, all that is required to determine the total power reflected off the satellite over the entire visible spectrum is to integrate under the resulting curves. Figure 20 shows the resulting curves for each of the materials selected for analysis. The results of computing the integrals (the total power reflected for full reflection off just one side at a time) are summarized in Table 11. The total efficiency of the reflection is computed by comparing the total power reflected to the total power that will be reflected for a perfect specular reflection.

Table 11: Total Power Reflected Off Select Materials

Material	Total Power Reflected (W)	Total Efficiency
Aluminized Kapton film	7.0	0.30
Aluminum	21.7	0.92
Gold	18.9	0.80
Silica under glass	5.0	0.21
Pyrolytic graphite	3.3	0.14

Because gravity-gradient booms only provide two axes of stabilization, the satellite is free to spin about the boom axis. This being the case, the chances of any one telescope viewing only one side of the target over the exposure time is small. Therefore, some extrapolation of the power spectrum received will be necessary to determine what side, or sides, of the satellite are visible during a given exposure period. Comparing data from two or more telescope sites viewing the same target simultaneously could aid in this goal. By comparing the power spectrum received at multiple locations, more could be learned about target orientation at that time period.
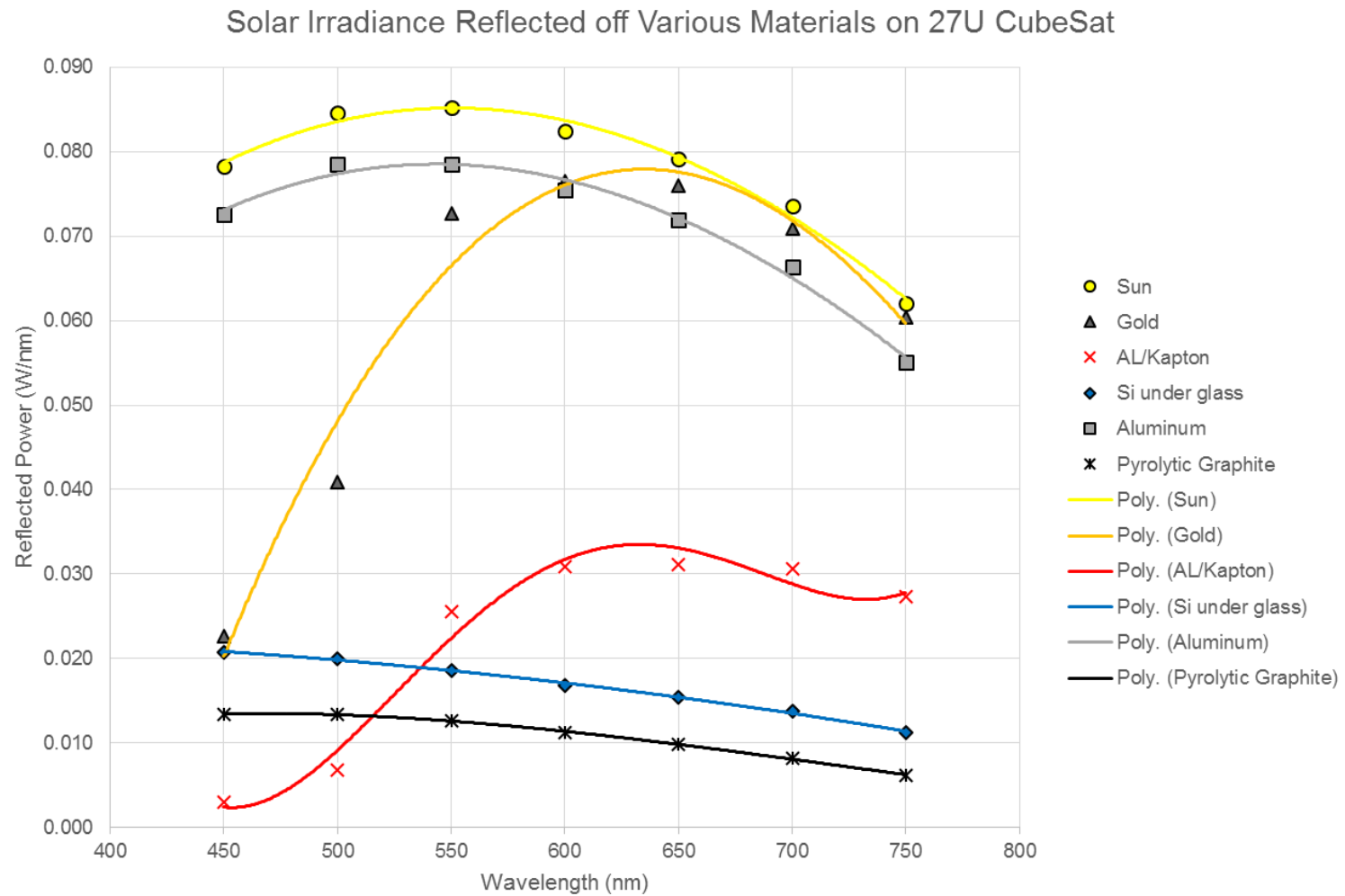
49

Figure 20: Power Reflected Off Various Materials on a 27U CubeSat

Chapter 6: Conclusions

Final Design Recommendation

The recommended initial calibration target for the FTN is a 27U CubeSat in a 450-km circular orbit inclined to at least 60°. The sides of the target are aluminum, aluminized Kapton film, pyrolytic graphite, and gold foil with two opposing sides covered in solar panels. From one of the solar panel ends, a gravity-gradient boom is deployed, providing two axes of passive pointing stability. The side panels of the satellite will fold out into a point to provide better reflection geometry. Future generations of designs will be based on the success or failure of this initial design. However, this initial design is relatively easy to manufacture and requires no post-launch personnel hours to command the satellite. The combination of these two things drive down the overall cost of the program, which benefits the program because the entire telescope network costs less than $2 million. It would not make sense, initially anyway, to design a calibration target that costs more than the rest of the program combined.

Recommendations for Future Work

Increasing numbers of researchers, particularly at universities, looking into utilizing CubeSats, which generally can be less expensive when compared to their full-sized counterparts. The greatest advantage to having a full ADCS and communication system available is the ability to control, measure, and communicate exact attitude data to the user on the ground. An actively controlled target for the purpose of calibrating the FTN could take on many forms. Because the satellite would have full power capabilities available to it, the possibilities are many. That being said, the first round design of an active control calibration target should probably be kept simple.

An initial design could have the same material scheme as the passively controlled target proposal with a gravity-gradient boom: gold, aluminized Kapton film, aluminum, and pyrolytic graphite with two opposing solar panels. Because there is more complexity to an active design, certain design constraints would force design changes in the panels, such as the addition of thermal regulation devices. The satellite would be able to maintain three-axis stabilization to varying degrees, depending on the attitude actuators chosen.

These actuators would allow the user on the ground to command the target to point in a certain manner when passing over a given site, allowing visibility of a single side, or a particular combination of sides, at any given time. The advantage of this type of control is that the observation data can be directly compared to the known orientation without having to extrapolate information about the satellite based on the power spectrum.

The most important area of research going forward will be more accurate modeling of the expected power spectra and various reflection scenarios. Understanding what the various power spectra received actually mean will be of critical importance to the program being a success. This modeling can be done before or after launch, but should be conducted before the data analysis phase of the mission.

Another important area of research will be more investigation into the materials for the side panels. While the chosen materials are stable in the space environment, there may be a better choice of materials from a reflectivity and/or distinguishability standpoint.

Finally, before development, more research will be needed into the exact length of the boom, and mass of the weight at the end of the boom, to optimize the passive control and pointing stability of the spacecraft.

References

[1]   USAF Academy Center for Space Situational Awareness, 2010, "Proposal for a Falcon Telescope Network," Colorado Springs, CO.

[2]   RC Optical Systems, 2013, "RCOS Carbon Truss 20 inch Ritchey-Chretien Telescopes." from http://www.rcopticalsystems.com/telescopes/20truss.html

[3]   Apogee Imaging Systems, 2013, "Alta F47." from http://www.ccd.com/pdf/Alta_F47.pdf

[4]   Krebs, D., 2014, "LCS 1, 2, 3, 4." Gunter's Space Page, from http://space.skyrocket.de/doc_sdat/lcs-1.htm

[5]   Encyclopedia Astronautica, n.d., "SURCAL." from http://www.astronautix.com/craft/surcal.htm

[6]   Bernhardt, P., Nichols, A., Thomas, L., Davis, M., Burris, R., Hoberman, C. and Davis, M., 2006, "Applications of the Precision Expandable Radar Calibration Target (PERCS) to Laser Imaging and Tracking Systems," *16th International Workshop on Laser Ranging*, Naval Research Laboratory.

[7]   National Aeronautics and Space Administration, n.d., "Starshine." from http://science.nasa.gov/missions/starshine/

[8]   California Polytechnic State University, 2009, "CubeSat Design Specification," Obispo, CA.

[9]   Puig-Suari, J., Schoos, J., Turner, C., Wagner, T., Connolly, R., and Block, R., 2000, "CubeSat Development and Cal Poly: The Standard Deployer and PolySat," Obispo, CA.

[10] Earth Observation Portal, n.d., "CubeSat Concept." from https://directory.eoportal.org/web/eoportal/satellite-missions/c-missions/cubesat-concept

[11] Pumpkin, 2013, "CubeSat Kit." from http://www.cubesatkit.com/content/design.html

[12] Krebs, D., 2014, "ALICE." Gunter's Space Page, from http://space.skyrocket.de/doc_sdat/alice.htm

[13] McHarg, M.G., 2014, Director of the Space Physics and Atmospheric Research Center, United States Air Force Academy, private communication.

[14] Dearborn, M., McHarg, G., and Andersen, G., n.d., "FalconSat-7." USAF Academy Center for Space Situational Awareness.

[15] Wertz, J.R., Everett, D.F., and Puschell, J.J., 2011, *Space Mission Engineering: The New SMAD*, Microcosm Press, Hawthorne, CA.

[16] National Earth Science Teachers Association, 2012, "Windows to the Universe." from http://www.windows2universe.org/earth/Magnetosphere/earth_magnetic_poles.html

[17] National Oceanic and Atmospheric Administration Space Weather Prediction Center, 2014, "Solar Cycle Prediction." from http://www.swpc.noaa.gov/SolarCycle/

[18] Sadraey, M., 2011, *Aircraft Performance:* Analysis, VDM Verlag Dr. Müller, Düsseldorf. Chap. 3.

[19] Gerhardt, D., and Palo, S., 2010, "Passive Magnetic Attitude Control for CubeSat Spacecraft," *24th Annual AIAA/USU Conference on Small Satellites*, AIAA, Logan, UT.

[20] Born, M., and Wolf, E., 1980, *Principles of Optics*, A. Wheaton and Co. Ltd, Exeter.

[21] Rayleigh Criterion, n.d., "Hyperphysics," from http://hyperphysics.phy-astr.gsu.edu/hbase/phyopt/imgpho/rayc.gif

[22] Ohio State University, n.d., "Astronomical Seeing and Adaptive Optics." from http://www.astronomy.ohio-state.edu/~martini/Astro890/Astro890L7.pdf

[23] Kane, T., 2014, Professor of Electrical Engineering and Meteorology, The Pennsylvania State University, private communication.

[24] Chun, F.K., 2014, Professor of Physics, United States Air Force Academy, private communication.

[25] Strobel, N., 2010, "Magnitude System," from http://www.astronomynotes.com/starprop/s4.htm

[26] King, L.B., and LaSarge, J.A., 2012, "The Oculus-ASR: An Orbiting Nanosatellite Testbed for Non-Resolved Object Characterization," *Advanced Maui Optical and Space Surveillance Technologies Conference*, Maui, HI.

[27] De Groh, K.K., Banks, B.A. Dever, J.A., Jaworske, D.A., Miller, S. K., Sechkar, E.A., and Panko, S.R., 2008, "NASA Glenn Research Center's Materials International Space Station Experiments (MISSE 1-7)," *International Symposium on 'SM/MpAC&SEED Experiment'*, Tsukuba.

[28] Dworak, D., Banks, B., Karniotis, C., and Soucek, M., 2006, "Evaluation of Protective Silicone/Siloxane Coatings in Simulated Low-Earth-Orbit Environment," Journal of Spacecraft and Rockets, 43(2), pp. 393-401.

[29] Photonics Media, 2014, "Photonics.com." from http://www.photonics.com/EDU/Handbook.aspx?AID=25501

[30] Harvey, G., n.d., "Optical-Witness-Plates Experiment Results," NASA Langley Research Center, Hampton, VA.

[31] Querry, M., 1985, "Optical Constants," ADA158623, U.S. Army Armament, Maryland, MD.

[32] Honsberg, C., and Bowden, S., n.d., "Anti-Reflection Coatings." from http://pveducation.org/pvcdrom/design/anti-reflection-coatings

[33] Chandler, C., n.d., "Radiation." from http://qdl.scs-inc.us/2ndParty/Pages/10522.html